

**UCLA**

**UCLA Electronic Theses and Dissertations**

**Title**

Effects of water chemistry on NF/RO membrane structure and performance

**Permalink**

<https://escholarship.org/uc/item/4rd663tt>

**Author**

Mo, Yibing

**Publication Date**

2013

Peer reviewed|Thesis/dissertation

UNIVERSITY OF CALIFORNIA

Los Angeles

Effects of Water Chemistry on  
NF/RO Membrane Structure and Performance

A thesis submitted in partial satisfaction  
of the requirements for the degree Master of Science  
in Civil Engineering

by

Yibing Mo

2013



## ABSTRACT OF THE THESIS

Effects of Water Chemistry on  
NF/RO Membrane Structure and Performance

by

Yibing Mo

Master of Science in Civil Engineering

University of California, Los Angeles, 2013

Professor Eric M.V. Hoek, Chair

In recent decades, there has been increasing concern about water contaminated by chemicals of emerging concern (CECs), a.k.a., trace organic micropollutants or emerging contaminants. Recent advances in analytical procedures enable detection of compounds like pharmaceuticals & personal care products (PhPCPs), hormones, endocrine disrupting compounds (EDCs), disinfection by-products (DBPs) and synthetic organic chemicals (SOCs). Many members of these compound classes are carcinogen or mutagens. A number of conventional and advanced methods have been evaluated (individually and in combination) for removal of CECs from water sources, including enhanced coagulation, activated carbon, activated sludge, membrane bioreactors, riverbank filtration, nanofiltration (NF), reverse osmosis (RO), and advanced

oxidation processes. NF and RO membranes can achieve very high removals of many CECs; however, removal of a specific solute by a given membrane can vary widely at different water treatment plants. It has been proposed that different membrane performances were due to variations in water chemistry (*i.e.*, pH, TDS, hardness, etc.), but it was not specified as to why the water chemistry so profoundly influences observed CEC removal. This study attempts to relate how water chemistry affects NF and RO membrane performance by elucidating structural changes in the membrane barrier layer solely due to background water chemistry – using model membranes, and well controlled laboratory studies using different solutes and electrolytes. A recently proposed NF/RO structure-performance model used to fit experimental data suggests that NF/RO membranes become looser (*i.e.*, lower rejection of trace organics and high water permeability) with increasing water ionic strength, pH and divalent content.

The thesis of Yibing Mo is approved

Shaily Mahendra

Michael K. Stenstrom

Eric M.V. Hoek, Committee Chair

University of California, Los Angeles

2013

## Table of contents

<b>1. Introduction.....</b>	<b>1</b>
1.1. Background, motivation, and significance.....	2
1.1.1. Drinking water.....	2
1.1.2. Chemicals of emerging concern (CEC).....	2
1.1.3. Removal processes.....	3
1.1.3.1. Granular activated carbon.....	3
1.1.3.2. Advanced oxidization process.....	4
1.1.3.3. NF/RO.....	5
1.2. Hypothesis and scope of work.....	6
<b>2. Review of past work.....</b>	<b>9</b>
2.1. Chemicals of emerging concern (CEC's) in drinking water.....	10
2.1.1. Classes of chemicals.....	10
2.1.1.1. Disinfection by-products.....	10
2.1.1.2. Pharmaceuticals & personal care products.....	12
2.1.1.3. Hormones & endocrine disruptors .....	13
2.1.1.4. Industrial solvents.....	14
2.1.2. Properties of CECs.....	16
2.2. Organic rejection mechanisms of NF/RO membranes.....	17
2.2.1. Steric exclusion.....	17
2.2.2. Solute-membrane-solution interaction.....	19
2.2.3. Donnan interactions.....	20
2.3. Effect of water chemistry on NF/RO membrane performance.....	21
2.3.1. Concentration.....	21
2.3.2. pH.....	21
2.3.3. Divalent ions.....	22

2.4.	Transport model development.....	23
2.4.1.	Classical solution-diffusion model.....	23
2.4.2.	Kedem-Kechalsky model.....	26
2.4.3.	Spiegler-Kedem model.....	27
<b>3.</b>	<b>Theory and Experiment.....</b>	<b>30</b>
3.1.	Extended solution-diffusion-convection (xSDC) Model.....	30
3.1.1.	Water transport.....	30
3.1.2.	Solute transport.....	32
3.1.3.	General description of xSDC model.....	33
3.2.	Membranes: NF90, NF270, and XLE.....	35
3.3.	Solutes: Ethylene Glycol and 1,4-dioxane.....	36
3.4.	Water chemistry: Concentration, pH, and divalent ions.....	37
3.5.	Analytic method.....	37
3.6.	Contact angle measurements.....	38
3.7.	Membrane surface tension parameters.....	38
3.8.	Performance testing.....	39
<b>4.</b>	<b>Result and Discussion.....</b>	<b>40</b>
4.1.	Membrane characterization.....	41
4.2.	Solute-membrane-solution interaction energy.....	43
4.3.	Performance test result for EG.....	45
4.3.1.	Effect of water chemistry on membrane water permeability .....	45
4.3.1.1.	Effect of ionic strength.....	45
4.3.1.2.	Effect of pH.....	46
4.3.1.3.	Effect of divalent ions.....	47
4.3.2.	Effect of water chemistry on EG rejection.....	49
4.3.2.1.	Effect of ionic strength.....	49
4.3.2.2.	Effect of pH.....	52



4.3.2.3. Effect of divalent ions.....	54
4.4. Membrane structural parameters obtained from EG.....	56
4.5. Real rejection and fitting results for 1,4-dioxane.....	57
4.5.1. Effect of ionic strength.....	60
4.5.2. Effect of pH.....	63
4.5.3. Effect of divalent ions.....	65
4.5.4. Fitting interaction energy analysis for 1,4-dioxane.....	67
<b>5. Conclusions.....</b>	<b>69</b>
<b>References.....</b>	<b>71</b>

## **List of Tables**

**Table 2.1.** Properties of chemicals of emerging concern.

**Table 3.1.** Physic-chemical properties of EG and 1,4-dioxane.

**Table 4.1.** Contact angle of membranes with Water, Diiodomethane and EG

**Table 4.2.** Surface tension parameters of solutes.

**Table 4.3.** Membrane surface tension parameters in ten water chemistries.

**Table 4.4.** Interaction energy of membrane-solute-water and membrane-water for EG.

**Table 4.5.** Interaction energy for 1,4-dioxane-membrane-water.

## List of Figures

**Figure 2.1.** Size exclusion effect on organic rejection by NF/RO membrane [1].

**Figure 2.2.** Solute-membrane-solution interaction effect on organic rejection by NF/RO membrane [1].

**Figure 2.3.** Donnan Exclusion effect on charged solute rejection by NF/RO membrane [1].

**Figure 3.1.** Combined effects of membrane structure factor, membrane pore size and water-membrane interaction energy on water permeability.

**Figure 3.2.** Combined effects of membrane structure factor, membrane pore size and solute-water-membrane interaction energy on solute rejection.

**Figure 3.3.** Chemical Structure of (a) Polyamide and (b) Poly piperazine.

**Figure 4.1.** Effect of ionic strength (NaCl) on membrane water permeability.

**Figure 4.2.** Effect of pH on membrane water permeability.

**Figure 4.3.** Effect of divalent ions on membrane water permeability.

**Figure 4.4.** Effect of ionic strength (NaCl) on EG rejection for NF90 (a), XLE (b), NF270 (c) membranes (5mM=red, 50mM=blue, 500mM=black).

**Figure 4.5.** Effect of pH on EG rejection for NF90 (a), XLE (b), NF270 (c) membrane (pH3=red, pH5=blue, pH7=green, pH9=pink, pH11=black).

**Figure 4.6.** Effect of divalent ions ( $Mg^{2+}$ ,  $Ca^{2+}$ ) on EG rejection for NF90 (a), XLE (b), and NF270 (c) membrane (50mM NaCl=red, 50mM  $CaCl_2$ =blue, 50mM  $MgCl_2$ =black).

**Figure 4.7.** Calculated membrane pore size (left, blue) and structural factor (right, red) for NF90 (a), XLE (b), and NF270 (c).

**Figure 4.8.** 1,4-dioxane real rejection and fitting rejection curves for NF90 (a), XLE (b), NF270 (c) under three concentrations (5 mM=red, 50 mM=blue, 500 mM=black).

**Figure 4.9.** 1,4-dioxane real rejection and fitting rejection curves for NF90 (a), XLE (b), NF270 (c) under five pH (pH3=red, pH5=blue, pH7=green, pH9=pink, pH11=black).

**Figure 4.10.** 1,4-dioxane real rejection and fitting rejection for NF90 (a), XLE (b), NF270 (c) under two divalent ions (50mM NaCl=red, 50mM CaCl<sub>2</sub>=blue, 50mM MgCl<sub>2</sub>=black).

## **ACKNOWLEDGEMENTS**

I would like to sincerely thank my advisor, Professor Eric M.V. Hoek, for being patient and encouraging. I also appreciate him for showing his kind concern about my future study and career.

I also would like to thank my committee members: Dr. Michael K. Stenstrom and Dr. Shaily Mahendra for their academic support and encouragement.

I also would like to thank our group members: Jinwen Wang, Maivs Wong, Marytheresa M Pendergast, Benjamin J Feinberg, Catalina Marambio Jones for their help and encouragement. Typically, I would like to thank Jinwen Wang for being patience, and gave me a lot of guide and help in experiment and data analysis.

Finally, I would like to thank my parents Wenlong Mo, Hexiang Dai in spiritual and financial support. Without your support, I could not finish my study. Also, I would like to thank God gave me wisdom and protected me throughout my master study in U.S.

**CHAPTER 1**  
**INTRODUCTION**

## **1. Introduction**

### **1.1. Background, Motivation, and Significance**

#### **1.1.1. Drinking water**

There are three basic guidelines in determining drinking water quality [2]: (1) the water must be free of disease causing bacteria, (2) the concentration of harmful chemicals are below acceptable levels and (3) the concentration of radioactive compounds are below defined thresholds. In recent decades, the drinking water industry has encountered great challenges from modern industrial and agricultural growth and development. A lot of synthetic pollutants have found their way into drinking water sources. Generally, an adult consumes about two liters of water per day, which is much larger (in volume or mass) than the daily consumption of solid food; hence, the health risks imposed by contaminated drinking water are very important.

#### **1.1.2. Chemicals of emerging concern (CEC)**

Trace organic compounds in drinking water mainly come from industrial solvents, personal care products, pharmaceuticals, disinfection by-products and pesticides. Typically, the most notorious trace organic contaminants are N-nitroso-dimethylamine (NDMA), chloroform, 1,4-dioxane, methyl tert-butyl ether (MTBE), benzene, ethylbenzene, toluene, xylenes, 17 $\beta$ -Estradiol, etc. NDMA has received special attention because of its carcinogenicity at low concentrations in drinking water (3 ng/L, CA) [3]. Recently, 1,4-dioxane has become increasingly of more concern as it is not readily degraded. It has been found in many places around the United States and is classified as a probable carcinogen [4]. 17 $\beta$ -Estradiol is a natural

hormone and has great impact on affecting the ecological cycle. It has been reported that concentrations beyond 1ng/L will have adverse effects on the reproductive system for male aquatic animals [5]. Since many effects of these trace organic compounds' have not yet been identified, it is important to remove trace organic compounds from drinking water to eliminate potential health risks.

### **1.1.3. Removal processes**

#### **1.1.3.1. Granular activated carbon**

Filtration using Granular Activated Carbon (GAC) is a common method in water treatment. GAC can remove a wide range of compounds, including odor and color causing compounds, disinfection byproducts (DBPs), natural organic matter (NOM) and other toxic compounds. Usually, GAC has been used in filtration and post-filtration adsorption in many water treatment plants. Babi, K. G. et al. [6] reported that post-filtration adsorption was more efficient than filtration adsorption in removal of Trihalomethanes (THMs), haloacetic acids (HAAs) and dissolved organic carbon (DOC) from water sources. The researchers also showed that GAC performs well initially (first 50 days), but the removal declines after 50 days and remains steady at 50% removal after 150 days. The removal increased after 200 days due to biodegradation since biofilms formed over time on GAC. The removal of THMs by GAC resulted in negative values, which means the GAC adsorption for THMs is not stable and some adsorbed solutes have the potential to be desorbed over time.



Kim, Jinkeun et al. [7] also indicated that breakthrough, the limited removal of solutes by the adsorbent, occurred after three months and remained around 10% removal for THMs in filtration-adsorption type GAC. But for HAAs, the removal decreased rapidly in the first three months and then increased to 90%, which is attributed to biodegradation. A combination of a membrane bioreactor (MBR) and GAC for dissolved organic carbon removal was proposed by Nguyen et al. [8]. In this research, GAC was a complementary part to the MBR because the MBR is not efficient in removing hydrophilic and persistent organic compounds, while GAC is efficient in removing hydrophilic compounds and able to retain persistent organics from water. The total removal of various compounds with wide range of  $\log K_{ow}$  were all around 99%. From the previous combined MBR and GAC study, it was concluded that GAC was not good in adsorbing hydrophobic organics ( $\log K_{ow} > 3.2$ ). From the discussion above, GAC alone is not sufficient for water treatment. Furthermore, GAC is expensive to use and requires regeneration to maintain continuously functional.

### **1.1.3.2. Advanced oxidization processes**

Advanced oxidization processes (AOPs) refers to using various methods to generate hydroxyl radicals ( $\cdot\text{OH}$ ), which indiscriminately abstract electrons from reduced organic or inorganic pollutants in water [9]. Ito et al. [10] found  $\text{O}_3/\text{UV}$ ,  $\text{O}_3/\text{H}_2\text{O}_2$ ,  $\text{H}_2\text{O}_2/\text{UV}$  and  $\text{O}_3\text{H}_2\text{O}_2/\text{UV}$  are effective combination of AOPs in DOC removal. The authors also pointed out that none of the AOP methods was effective at complete mineralization of DOC, but they did contribute to

their subsequent biodegradability. Broseus et al. [11] showed that ozone based AOPs effectively removed pharmaceuticals, endocrine disruptors and pesticides, but ozone application is limited due to the formation of bromoform when wastewater contains bromide and NOM [12]. Plumlee et al. [13] used UV and reverse osmosis (RO) to investigate the NDMA removal and found that the application of UV within a range of 175-225 nm enhanced NDMA removal by breaking down the nitrogen-nitrogen bond. However, using UV method to remove NDMA is extremely expensive. For example, Cryptosporidium destruction requires a density of 8–12 mJ/cm<sup>2</sup>, but NDMA destruction may require a density of 600–800 mJ/cm<sup>2</sup> to achieve satisfactory removal [14]. Kruithof et al. [15] indicated that NDMA can be mainly removed by UV, while 1,4-dioxane can only be removed by hydroxyl radicals. Generally, AOPs can be effective in removing DOC and COCs, but they are energy intensive and expensive.

### **1.1.3.3. Nanofiltration and Reverse Osmosis**

Nanofiltration (NF) and RO are novel water treatment technologies that have been widely used in the industry of potable water and seawater desalination. NF/RO are effective processes to remove DOC for compounds larger than the characteristic membrane pore size [16]. The parameter  $\lambda$  ( $= r_s/r_p$ ) is used to characterize the solute-to-membrane pore size ratio. Yoon et al. [16] empirically found that rejection of organics was over 75% when  $\lambda$  was over 0.8. Besides  $\lambda$ , there are other factors that can influence NF/RO rejection of DOCs. From the solute perspective, factors like molecular weight, molecular size, acid disassociation constant ( $pKa$ ), hydrophobicity

( $\log K_{ow}$ ), and diffusion coefficient, etc. also affects how well removed it is. In terms of the membrane, parameters like molecular weight cut off (MWCO), membrane pore size, membrane thickness, membrane porosity, membrane surface charge, hydrophobicity, and membrane surface roughness, etc. will affect rejection of solutes. The feed water chemistry affects the rejection of solutes, including solution pH, ionic strength, hardness, total dissolved solute (TDS) [17]. Temperature also affects membrane performance through solute diffusivity and membrane swelling [18]. Hurwitz et al. [19] indicated that with increasing pH, salinity and presence of divalent cation, the polyamide membrane became more wetting, less hydrophobic and more electro-donor functionalized. Verliefde et al. [20] pointed out that hydrophilic solute tends to be highly rejected by hydrophobic membrane because of a low partition coefficient. Verliefde et al. [21] also showed that negatively charged organics could be highly rejected by NF/RO membrane because of negatively charged membrane surface. However, NF/RO membranes can only moderately remove trace organics in economic operating conditions [17]. Also, it has been reported that the same membranes exhibited different performances in different water chemistries [22].

## **1.2. Hypothesis and scope of work**

It is hypothesized that the background water chemistry changes the membrane free volume and inter-connectedness of the free volume due to swelling and deswelling caused by differences in salinity, pH, and divalent ions. In a series of studies, Nghiem et al. [23] showed that increasing pH from 6 to 8 increased NDMA rejection from 35% to 45%. Also, when the ionic strength of

feed water increased from 26 to 260 mM NDMA rejection decreased from 52% to 34%. They considered that high pH affects the charge of the functional groups in the membrane, and thus, change the membrane matrix formation (*i.e.*, pore size and porosity). They also suggested that high salinity increases the membrane pore size based on decreased rejection. Elimelech et al. [24] indicated that pH effect on membrane performance is due to electrostatic repulsion, membrane pore size and volume.

Analogously, membrane pore size and membrane structure parameters (*i.e.*, thickness, porosity) play important roles in membrane performance. It is logical to assume that membrane pore size  $r_p$  and membrane structure factor  $\Delta x/\varepsilon$  will change simultaneously because once the membrane pore size enlarged, the membrane thickness and porosity would increase as well. However, the pore size and the membrane structure parameter will have counter effects on the membrane performance; large membrane pore size increases water permeability and decreases solute rejection, while large membrane structure parameter decreases water permeability and increases solute rejection. To precisely characterize membrane structure, these two parameters have to be taken into consideration. Verliefde et al. [20] predicated membrane pore size through Spiegler-Kedem equation, but only used one equation to fit two unknowns producing somewhat arbitrary results. The first objective of this thesis is to develop a robust, but facile model relating membrane structure to observed separation performance. The second objective is to use the model to analyze experimentally determined water flux and solute rejection data obtained with different membranes in different water chemistries. The third objective is to apply the model to predict rejection of other solutes and compare to experimental results.

In addition to testing the stated hypothesis, the broader implication of this research is an improved, fundamental understanding of the relationship between observed separation performance and NF/RO membrane structure and physico-chemical properties. Chapter 2 comprises an extensive literature review of CECs in drinking water, membrane transport mechanisms, and classical membrane transport models. The literature review includes major organic solutes that are CECs in drinking water, effects of water chemistry on NF/RO performance, organic solute transport mechanisms and NF/RO transport model development history. Chapter 3 is a detailed description of experimental materials, methods as well as the derivation of a new NF/RO membrane structure-performance model. Chapter 4 discusses the experimental results interpreted through the structure-performance model and prediction results for 1,4-dioxane. Chapter 5 is a brief summary of major findings from this work and a description of future research.

**CHAPTER 2**  
**REVIEW OF PAST WORK**

## **2. Review of past work**

### **2.1. Chemicals of emerging concern (CEC) in drinking water**

There are four major groups of CECs: Disinfection by products (DBPs), Pharmaceuticals & personal care products (PPCPs), Endocrine disruptors (EDC) and industrial solvents. Most known industrial solvents and DBPs already have maximum contaminant limits (MCLs) or some type of action/notification levels defined by the US EPA. However, most chemicals in PPCPs and EDC groups are listed in Containment Candidate List (CCL), which means they are candidates for US EPA regulation.

#### **2.1.1. Classes of chemicals**

##### **2.1.1.1. Disinfection by-products**

DBPs are classified as carcinogens or mutagens, which prevents water to be reused and poses health risks to drinking water sources. Reuse water always contains a large amount of NOMs, which is a prerequisite for DBPs' formation during the disinfection process. DBPs are also big issues for municipal tap water system since DBPs formation cannot be avoided in the distribution system from the drinking water plant to consumers' tap [25]. THMs, HAAs, haloacetonitriles (HANs), Haloketones (HKs), haloketones (HKs), chloral hydrate (CH), cyanogen chloride (CNCl), chloropicrin (CP), and NDMA are common DBPs formed during the disinfection process in wastewater treatment plants when chlorine or chloramine disinfectants reacts with NOMs [12, 26, 27]. THMs, HAAs and NDMA are emerging DBPs that have been widely studied.

Group of THMs contains four compounds: Chloroform (TCM), Bromodichloromethane (BDCM), Dibromochloromethane (TBM), and Bromoform (DBCM). Bromoform could also be formed through the ozone disinfection process [12]. TCM is the dominant compound of THMs when bromide concentration is low [28]. Inhalation, ingestion and skin penetration are the major pathways for intake of chloroform that can adversely affect people's health. Chlorinated drinking water is the largest source of human exposure to THMs. Bathing and swimming in chlorinated water also increases people's exposure to chloroform. Chloroform has been used as an inhalation anesthetic, which means it has effects on the central nervous system. Additionally, experiments on animals have indicated that high concentration of chloroform is toxic to the liver and kidney. The U.S. EPA has classified chloroform as a probable carcinogen according to studies and has set a maximum concentration level (MCL) of 80 ppb for THMs in drinking water. The MCLs are 70 ppb for TCM, 60 ppb for DBCM, 0.6 ppb for BDCM and 5 ppb for Bromoform [29, 30].

HAAs consists of nine species: there are monochloroacetic acid (MCAA), dichloroacetic acid (DCAA), and trichloroacetic acid (TCAA); monobromoacetic acid (MBAA), dibromoacetic acid (DBAA), and tribromoacetic acid (TBAA); bromochloroacetic acid (BCAA), bromodichloroacetic acid (BDCAA), and chlorodibromoacetic acid (CDBAA) [12]. HAAs are formed through the reaction of chlorine and NOMs in raw water. Typically, HAAs are also called HAA5 because only five compounds are prevalent (DCAA, TCAA, MCAA, MBAA and DBAA). Long time of drinking chlorinated water may increase the risk of getting cancer. EPA has established a MCL of 60 ppb for HAAs [12, 30], single MCL of 20 ppb for TCAA, and single MCL of 70 ppb for MCAA [30].



NDMA is one species of nitrosamines, which are carcinogenic, mutagenic and teratogenic [31]. It was used as an additive for liquid rocket fuel, but now NDMA is a by-product. It has been found in many environments, such as cigarette smoke, rocket launch fields, food and drinking water [32]. Animal studies showed that NDMA has significant effect on tumor occurrence among different species through oral, inhalation and other exposure [32]. In 1998, NDMA was first detected in a drinking water well in Northern California. Then more and more places in California detected NDMA in their drinking water sources. In 2006, a Public Health Goal (PHG) of 0.003  $\mu\text{g/L}$  for NDMA was proposed by the Office of Environmental Health Hazard Assessment (OEHHA) based on one in million lifetime cancer risk [32]. NDMA is not currently regulated by the EPA, but there is a notification level of 0.01  $\mu\text{g/L}$  and response level of 0.3  $\mu\text{g/L}$  [3]. U.S. EPA has classified NDMA as a probable carcinogen and published a cancer risk level of 0.7  $\text{ng/L}$  [33]. NDMA has been listed on the CCL [34], which means it is a good candidate for EPA regulation [32].

#### **2.1.1.2. Pharmaceuticals & personal care products**

PPCPs have been largely consumed by people in recent decades and over 3000 different compounds have been used worldwide for various medical and cosmetic purposes [35]. PPCPs in the environment come from anthropogenic sources, including residues from pharmaceutical manufacturing plants, hospitals, illicit drugs use, veterinary drug use and agribusiness [36]. Representative compounds of emerging for PPCPs are antibiotics, lip-regulator, anti-inflammatories, anti-epileptics and X-ray contrast media [37]. Some PPCPs can be easily

degraded, but some are inert due to its chemical stability. Lipophilic compounds tend to stay in body, retained in fat, while hydrophilic compounds will be excreted to the environment through urine and sweat, increasing its concentration in water sources [35]. Currently, there is no direct evidence to prove that PPCPs have adverse effect on human health through drinking water, therefore EPA does not regulate PPCPs [36].

### **2.1.1.3. Hormones & endocrine disruptors**

EDCs have been detected at many places in the world, EDCs constitute of various compounds, including synthetic, natural hormones and their derived forms, and hormone-like compounds from different fields (*i.e.*, PPCPs, pesticides, plasticizers, antioxidants, disinfections) [38]. Natural hormones comprise progestogens, glucocorticoids, mineralocorticoids, androgen and estrogens. Estrogens mainly consist of female steroids (*i.e.*, estradiol, estrone and estriol), which have been widely studied due to its adverse effect on male aquatic animals [5]. Hansen et al. [39] revealed that 1ng/L of 17 $\beta$ -Estradiol has obvious induction of vitellogenin for trout, which means EDCs can affect fish at very low concentrations. However, the impacts on human health are still controversial, complicated and has limited research due to regulations [40]. Sharpe R. M. et al. [41] showed that diethylstilbestrol as an orally active synthetic non-steroidal estrogen may cause sperm decrease in human males. EPA have not listed any EDCs as controlled chemicals in drinking water due to the limited correlative evidence received, but EPA have put 17 $\alpha$ -Estradiol, 17 $\beta$ -Estradiol, Estriol, Estrone and synthetic steroids (Ethinyl Estradiol, Mestranol) into CCL as regulated candidates [34].

#### **2.1.1.4. Industrial solvents**

Industrial solvents is a large group, including emerging categories of Polychlorinated Biphenyl, BTEX and poly-aromatic hydrocarbons. PCBs are made up of different individual chlorinated biphenyl components. PCBs were once widely produced during 1929 to 1979. After 1979, commercial production of PCBs was banned because of its toxicity and stability to degradation. PCBs can accumulate in plants and animal's body, which means higher concentration is found higher up in the food chain. Research showed that PCBs have adverse effects on the endocrine system, nervous system and reproductive system, and have been classified as a probable carcinogen based on an animal cancer study [42].

BTEX is an acronym standing for benzene, ethylbenzene, toluene and xylenes. BTEX is notorious due to its volatility, stability, high carcinogenicity, and other adverse effects on human health. BTEX is a part of crude oil that has been widely detected around petroleum and natural gas production sites, gas stations, and underground storage tanks. Also, BTEX in the air is another big threat to people who live in big cities. Zhang et al. [43] have reported that the atmospheric concentrations of BTEX in Beijing were 27.2, 31.9, 23.2, 19.1  $\mu\text{g}/\text{m}^3$  in autumn, winter, spring, and summer, respectively. The World Health Organization (WHO) estimated that the life time exposure to  $1\mu\text{g}/\text{m}^3$  of BTEX would cause 6 cases of leukemia per 1,000,000 people [44]. EPA have defined MCLs of BTEX concentration in drinking water of 7 ppb, 700 ppb, 1ppm, 10 ppm, respectively [45].

PAHs have been found at oil and coal related places, like gas stations, oil production sites, coal gasifications, iron and steel fields. Also, PAHs are byproducts of barbecue grills and stoves

caused by high temperature cooking. Cigarette smoke is another major source for individual exposure [46]. EPA and WHO have identified PAHs as carcinogens, mutagens and teratogens. EPA has regulated some PAHs in the drinking water, but only Benzo-a-pyrene has a MCL of 0.2 ppb. Some of PAHs are classified as probable carcinogens, like Benz-a-anthracene, Benzo-a-pyrene, Benzo-b-fluoranthene, Benzo-k-fluoranthene and Indeno-1,2,3,-c,d-pyrene but without MCL [45].

## 2.1.2. Properties of CEC's

**Table 2.1.** Properties of chemicals of emerging concern.

Organic names and shorts	Groups	Chemical formula	MW (g/mol)	$r_s^{[20]}$ (nm)	$D_\infty^{[47]}$ ( $\times 10^{-5}$ cm <sup>2</sup> /s)	log Kow	Henry's law constant (M/atm)	MCLs for drinking water <sup>[45]</sup> (ppb)
<b>1,4-Dioxane [4]</b>	Industrial	C <sub>4</sub> H <sub>8</sub> O <sub>2</sub>	88.1	0.21	1.00	-0.27	200	NA
<b>TCE**</b>	Industrial	C <sub>2</sub> HCl <sub>3</sub>	131.4	0.23	0.91	2.6	0.11	5
<b>MTBE** [48]</b>	Industrial	C <sub>5</sub> H <sub>12</sub> O	88.2	0.27	0.78	1.24	1.6	20-40
<b>Phenol*</b>	Industrial	C <sub>6</sub> H <sub>6</sub> O	94.1	0.23	0.91	1.46	2900	300
<b>Benzene** [49]</b>	Industrial	C <sub>6</sub> H <sub>6</sub>	78.1	0.21	0.98	2.13	0.18	1
<b>Toluene** [49]</b>	Industrial	C <sub>7</sub> H <sub>8</sub>	92.14	0.25	0.86	2.73	0.15	1000
<b>Ethylbenzene**</b>	Industrial	C <sub>8</sub> H <sub>10</sub>	106.2	0.27	0.78	3.15	0.13	700
<b>Xylenes** [49]</b>	Industrial	C <sub>8</sub> H <sub>10</sub>	106.2	0.27	0.78	3.2	0.13	10000
<b>NDMA</b>	DBPs	C <sub>2</sub> H <sub>6</sub> N <sub>2</sub> O	74.1	0.21	0.99	-0.6	3850	0.007
<b>Chloroform**</b>	DBPs	C <sub>2</sub> HCl <sub>3</sub>	119.4	0.21	1.00	1.92	0.27	10
<b>Estrone [50]</b>	Hormone	C <sub>18</sub> H <sub>22</sub> O <sub>2</sub>	270.4	0.4	0.54	3.43	2.6 $\times 10^6$	NA
<b>17<math>\beta</math>-estradiol [50]</b>	Hormone	C <sub>18</sub> H <sub>24</sub> O <sub>2</sub>	272.38	NA	NA	4.01	2.78 $\times 10^7$	NA
<b>Estriol [50]</b>	Hormone	C <sub>18</sub> H <sub>24</sub> O <sub>3</sub>	288.4	NA	NA	2.81	7.6 $\times 10^8$	NA
<b>Bisphenol-A*</b>	Hormone	C <sub>15</sub> H <sub>16</sub> O <sub>2</sub>	228.3	0.36	0.59	3.3	10 <sup>6</sup>	50

\* Solid form under room temperature

\*\* Volatile in water

## **2.2. Organic rejection mechanisms of NF/RO membranes**

Many membranes have been developed and used for different purposes, especially in wastewater treatment and water purification applications.. Yoon et al. [16] found that rejection of organics was over 75% when  $\lambda$  was over 0.8 empirically, which indicated that solute size and membrane pore size plays an important role in membrane performance. Verliefde et al. [21] showed that steric exclusion could be affected by hydrophobic interactions between membrane and solute. It was further suggested that hydrophobic solutes could diffuse into hydrophobic membranes more easily than hydrophilic solutes even with the same solute size, thus resulting in low rejection of the hydrophobic solute than the hydrophilic solute. Kimura et al. [51] pointed out that negatively charged organic compounds were highly (>90%) rejected by negatively charged NF membrane because of the electrostatic repulsion, while positively charged organic compounds were rejected less than negatively charged organic due to electrostatic attraction. In conclusion, membrane rejection mechanisms can be classified into three components: steric exclusion, solute-membrane interaction and Donnan exclusion as described in the following sections.

### **2.2.1. Steric exclusion**

Steric exclusion refers to the physical barrier imposed by the membrane structural matrix and solute size. Solute with larger size than membrane pore size can be effectively removed [21]. The mechanism is shown in Figure 2.1. The solute size can be defined in different ways such as

stokes radius and geometric radius. The Stokes Einstein equation is obtained from classical thermodynamic and continuum flow mechanics describing the movement of spherical solute in a liquid [52], which assumes that the solute is spherical when calculating the stokes radius. In fact, some compounds, cannot be precisely described by stokes' radius, due to deviations from being spherical in shapes such as being long chain, elliptical, cubic and flat. Different shapes can be reflected in the diffusion coefficient in water. For example, long chain solute has low diffusion coefficient than short chain solutes. However, diffusion coefficients do not directly reflect shape of solute. Thus, the assumption of stokes equation is not accurate in describing the actual molecule size. Jose [52] revealed that using the stokes' radius as molecule size failed to predict the rejection for long chain compounds (*i.e.*, n-alcohols), but was reasonable for short chain compounds (*i.e.*, di-alcohols).

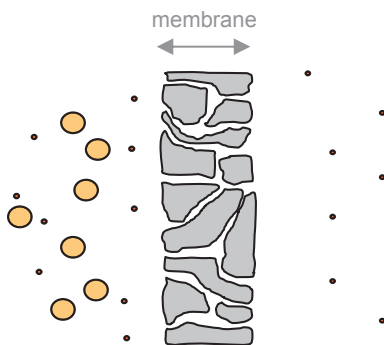


**Figure 2.1.** Size exclusion effect on organic rejection by NF/RO membrane [1].

### 2.2.2. Solute-membrane-solution interaction

Solute-membrane-solution interaction energy is an indicator to describe the interaction energy between solute, membrane and solution, which is described in Figure 2.3. The solute-membrane-solution interaction will be evident only when the solute size is close to the membrane pore size. If the solute size is too big, the solute will be fully rejected; if the solute size is too small, the solute is able permeate through the membrane quickly. Hydrophobic solutes can easily dissolve into hydrophobic solutions. When the hydrophobicity of the solute is high, the rejection of solute is low because of the solute partition effect. The mechanisms for solute-membrane-solution interaction proceeds in the following order: adsorption, formation of hydrogen bond (Van der Waals) and desorption as depicted in Figure 2.2.

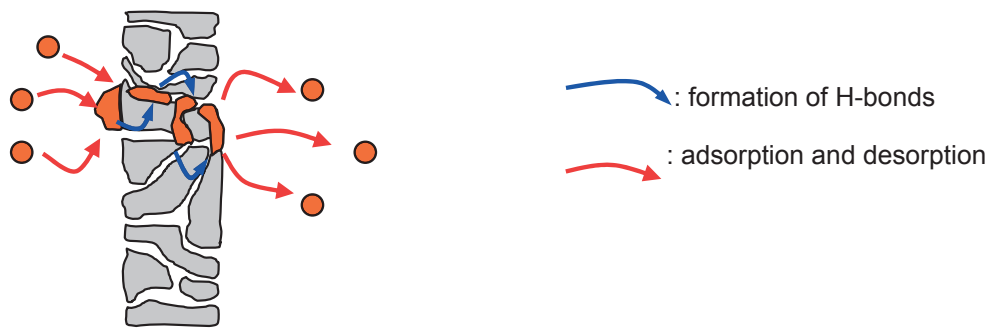


**Figure 2.2.** Solute-membrane-solution interaction effect on organic rejection by NF/RO membrane [1].



### 2.2.3. Donnan exclusion

Most NF/RO membranes are negatively charged due to polymer deprotonation. The most common membrane surface coating material used in NF/RO is polyamide, which has a pKa of  $5.7 \pm 0.3$  [53]. Under common water chemistry, the functional group of polyamide is carboxyl which will disassociate by releasing one hydrogen ion, causing the membrane surface to be negatively charged. Negatively charged membrane repels negatively charged matters (*i.e.*, NOM, chloride ion, etc.) and attracts positively charged matters (*i.e.*, sodium, magnesium, calcium, etc.). Co-ions can be highly rejected while counter-ions tend to transport into membrane phase. This phenomenon is vividly described in Figure 3.2. The partition coefficient of ions plays an important role in Donnan exclusion due to unevenly distributed concentrations of ions in the membrane phase and in the bulk phase. The concentration difference of ions between the bulk and the membrane result in a Donnan potential, which is an indicator of the partition extent for charged solute and membrane surface charge density [54].

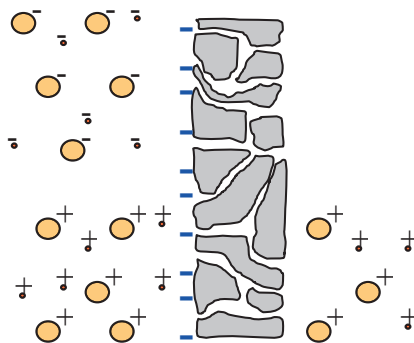


**Figure 2.3.** Donnan Exclusion effect on charged solute rejection by NF/RO membrane [1].

## **2.3. Effect of water chemistry on NF/RO membrane performance**

### **2.3.1. Concentration**

Concentration is an important factor in determining NF/RO membrane performance, because it generates osmotic pressure, which will go against the applied hydraulic pressure and lower the water permeability. Based on classical diffusion theory, no matter how concentration changes, salt rejection is not affected as that it is intrinsic to the membrane. However, Oo et al. [55] reported that the removal of boron decreased by 20% as the concentration of NaCl increased from 2 g/L to 14 g/L in the feed solution. Nghiem et al. [23] observed that as ionic strength increased from 26mM to 260mM for NaCl solution, the rejection of NDMA decreased from 52% to 34%. It was attributed to high ionic strength swelling the membrane, increasing the pore size and thus, reducing NDMA rejection. As discussed above, it is clear that concentration of salt has moderate impact on membrane performance.

### **2.3.2. pH**

As discussed in the previous section, most commercial NF/RO membranes are made of polyamide. Thus, when NF/RO membranes are immersed in water, the predominant carboxyl groups of polyamide will deprotonate, causing the membrane surface to be negatively charged. Different pH will result in different surface charges because of different deprotonation degrees. Previous study conducted by Yang et al. [56] revealed that as pH increased, the polyamide membrane surface charge decreased because of the dissociation of carboxyl group. The contact angle of solution on the membrane also decreased as pH increased, which means that the

membrane became more hydrophilic at high pH. The same phenomenon was also observed by Hurwitz et al. [19] that the contact angle decreased as pH increased, and the membrane surface became more hydrophilic. Hoang et al. [57] further pointed out that rejection of  $\text{Cl}^-$  increased as pH increased from 3 to 8, and ion rejection reached a minimum when pH was around 5. He indicated that the nadir point was due to the membrane surface charge being neutral at that pH, which is also known as the pKa for that specific membrane. Water permeability was only slightly affected by pH within that range. NDMA is an uncharged organic; the rejection of NDMA is only governed by membrane pore size and its own hydrophobicity. Theoretically, if pH does not affect membrane structure, the rejection of NDMA should not be affected by membrane surface charge change due to pH either. However, Nghiem et al. [23] found that N-nitrosamine rejection by TFC-HR membrane decreased as pH decreased from 9 to 3.5.

### **2.3.3. Divalent ions**

Typical divalent ions like  $\text{Ca}^{2+}$  and  $\text{Mg}^{2+}$  are commonly found in natural waters, like ground water and seawater. Hurwitz et al. [19] reported that  $\text{Ca}^{2+}$  and  $\text{Mg}^{2+}$  make the membrane more hydrophilic due to increased attraction to water molecules and in helping water molecules become more oriented. Bartels et al. [58] indicated that divalent ions will shield the membrane surface charge and reduce the Donnan potential, which means membrane surface charge will be reduced at the presence of divalent ions. Jin et al. [59] showed that  $\text{Ca}^{2+}$  and  $\text{Mg}^{2+}$  contributed to hardness in water and will tend to form scalants on the membrane surface if exceeding the solubility limits of certain ionic compounds, and thus reducing water permeability. If the

membrane surface continues to accumulate divalent ions, the membrane surface charge would be changed to positive value at high ionic strength.

## **2.4. Transport model development**

Many mathematical models have been developed to characterize the transport mechanisms of NF/RO membranes. Model simulation is important to membrane understanding, application and development. With the help of models, the membrane transport theory could be better understood and better performing membranes could be developed. NF/RO models can be separated into three groups based on different assumptions: irreversible thermodynamics models (*i.e.*, Kedem-Katchalsky and Spiegler-kedem models); nonporous or homogenous model (*i.e.*, solution diffusion, solution diffusion convection models); and pore flow models (*i.e.*, Hagen-Poiseuille, Kozeny Carman models). Some models also include the electrostatic effect to describe the relationship between charged membranes and charged solutes [60].

### **2.4.1. Classical solution-diffusion model**

NF/RO membranes are considered as nonporous membranes, and the main mechanism for solution and solute to pass through the membrane is by diffusion. Lonsdale developed the classical solution diffusion model (SD) in 1965. The SD model is based on the following assumptions: 1) Solute and solution diffusion both occurs across the nonporous membrane; 2) Diffusion for solute and solution are separate and driven by its own chemical potential gradient across the membrane; 3) The chemical potential gradient is determined by the concentration

difference and pressure difference across the membrane [60].

SD model is developed based on Fick's law, which assumes the flux of water is only governed by diffusion. The equation of Fick's law is expressed as

$$J_i = -D_i \frac{dC_i}{dz} \quad \text{Eqn (1)}$$

where  $dC_i/dz$  is the concentration gradient of solution  $i$  across the membrane,  $D_i$  is the diffusivity in the membrane. According to Henry's law, the chemical potential gradient for water is expressed as

$$\mu_w = \mu^0 + RT \cdot \ln\left(\frac{C_w}{C_0}\right) \quad \text{Eqn (2)}$$

where  $C_w$  is the water concentration in membrane and  $C_0$  is 1mol/L. After taking the derivative of both sides, the expression becomes

$$d\mu_w = -RT \cdot \left(\frac{dC_w}{C_w}\right) \quad \text{Eqn (3)}$$

Substituting Eqn (3) into Eqn (1), yields

$$J_w = \frac{D_{wm} C_{wm}}{RT} \frac{d\mu_w}{dz} \approx \frac{D_{wm} C_{wm}}{RT} \frac{\Delta\mu_w}{\Delta x} \quad \text{Eqn (4)}$$

where  $\Delta x$  is the membrane thickness. Membrane water chemical potential change is expressed as

$$\Delta\mu_w = RT \cdot \ln(\Delta C_w) + V_w \cdot \Delta P \quad \text{Eqn (5)}$$

where  $V_i$  is solution molar volume. The osmotic pressure of a solution at a certain concentration,

$C_w$  can be expressed as

$$\pi = \frac{-RT}{V_w} \ln(C_w) \quad \text{Eqn (6)}$$

After integrating equations Eqn (6) and Eqn (5), the membrane water chemical potential becomes

$$\Delta\mu_w = -V_w \cdot \pi + V_w \cdot \Delta P \quad \text{Eqn (7)}$$

Combining Eqn (7) and Eqn (4) gives the final expression for solution flux,

$$J_w = \frac{D_{wm} C_{mw} V_w}{RT \Delta x} (\Delta P - \Delta \pi) = A(\Delta P - \Delta \pi) = \left[ \frac{\text{mol}}{\text{m}^2 \text{s}} \right] \quad \text{Eqn (8)}$$

Classical diffusion model assumes solute flux is not driven by pressure difference, but driven by a solute concentration difference, or

$$J_s = -D_{sm} \frac{dC_{sm}}{dz} \approx D_{sm} \frac{\Delta C_{sm}}{\Delta x} \quad \text{Eqn (9)}$$

Where  $\Delta C_{sm}$  is the concentration difference across the membrane,  $D_{sm}$  is the diffusion coefficient in the membrane matrix. The concentration in the membrane can be related to the feed and permeate concentration times a partition coefficient  $K_{sm}$  and the final solute flux equation is expressed as

$$J_s = \frac{D_{sm} K_{sm}}{\Delta x} (C_F - C_P) = B(C_F - C_P) = \left[ \frac{\text{mol}}{\text{m}^2 \text{s}} \right] \quad \text{Eqn (10)}$$

Where  $B$  refers to solute permeability, by combining Eqn (10) and Eqn (8), gives

$$J_s = B \cdot \Delta C = J_w \cdot C_p \quad \text{Eqn (11)}$$

$$\frac{B \cdot (C_F - C_P)}{C_F} = J_w \cdot \frac{C_P}{C_F} = J_w \cdot \frac{(C_P - C_F) + C_F}{C_F} \quad \text{Eqn (12)}$$

$$\frac{(C_F - C_P)}{C_F} = \text{Rejection} \quad \text{Eqn (13)}$$

After substitution, Eqn (12) can be written as

$$R = \frac{J_w}{J_w + B} \quad \text{Eqn (14)}$$

The benefit of this model is that only two parameters need to be characterized, water permeability ( $A$ ) and salt permeability ( $B$ ). This classical model has been used widely in

determining salt rejection and organic rejection of membranes. But Mazid [61] indicated that SD model is limited for many RO membranes because of imperfections in commercial RO membranes, which means that mass transport occurs is not only by diffusion, but also by convection. In addition, SD model does not account for concentration polarization, the buildup of salt at the membrane surface, which occurs in real operating conditions.

#### 2.4.2. Kedem-Kechalsky model

Kedem-Kechalsky model (KK) was developed based on linear irreversible thermodynamics. The model is based on the assumption that the membrane system is close to equilibrium, and that the system can be viewed as an assembly of small local equilibriums. However KK model is limited to membrane systems with two-component solutions; a diluted solution and a well stirred condition [62]. KK model defines  $J_w$  as a function of applied pressure and osmotic pressure, and written as [62]

$$J_w = A(\Delta P - \sigma \Delta \pi) \quad \text{Eqn (15)}$$

$$J_s = B \Delta \pi + (1 - \sigma) C_{avg} J_w \quad \text{Eqn (16)}$$

where  $A$  is water permeability,  $B$  is solute permeability, and  $\sigma$  is reflection coefficient.  $C_{avg}$  is the averaged concentration of membrane of feed side and permeate side.  $\Delta \pi$  is the osmotic pressure difference defined as

$$\Delta \pi = RT(\Delta C) \quad \text{Eqn (17)}$$

Some important parameters like  $A$ ,  $B$  and  $\sigma$  in the KK model are expressed as

$$A = \frac{J_v}{\Delta P_{\pi=0}} \quad \text{Eqn (18)}$$

$$B = \frac{\Delta P}{\Delta \pi_{Jv=0}} \quad \text{Eqn (19)}$$

$$\sigma = \frac{J_s}{\Delta \pi_{Jv=0}} \quad \text{Eqn (20)}$$

when the  $\sigma$  equals to 1, the membrane is fully rejecting allowing only solution to pass through membrane and fully rejecting solute. When the  $\sigma$  equals to 0, membrane is nonselective.

Since KK model considers the membrane filtration process as a black box, it can be used for any kind of membrane. Kovacs et al. [63] applied KK model to calculate the permeate flux and rejection of diprotic amino acid compounds by NF membrane with satisfactory accuracy. Maria et al. [64] found that the water permeability decreased as the concentration of ethyl alcohol and glucose increased. The drawback to this model is that the coefficients have a dependence on concentration, therefore, Spiegler and Kedem developed another model called Spiegler-Kedem model to overcome this disadvantage.

### 2.4.3. Spiegler-Kedem model

The Spiegler-Kedem model (SK) is developed on the foundation of the KK model and irreversible thermodynamics. The main difference between SK and KK is that the SK model normalized the water permeability and salt permeability to the membrane thickness. The SK model is expressed as [65]



$$J_w = \frac{A_i}{dx} (dP - \sigma d\pi) \quad \text{Eqn (21)}$$

$$J_s = P\Delta x \frac{dC}{dx} + (1 - \sigma)C_{avg}J_w \quad \text{Eqn (22)}$$

where  $A_i$  is intrinsic membrane permeability,  $dx$  represents local distance of membrane thickness,  $P$  is local solute permeability. Eqn (22) can be integrated across the membrane to yield [66]

$$R_{real} = 1 - \frac{C_p}{C_m} = \sigma \frac{1 - F}{1 - \sigma F} \quad \text{Eqn (23)}$$

$$F = \exp(-J_w A) = \exp\left(-\frac{J_w(1 - \sigma)}{B}\right) \quad \text{Eqn (24)}$$

After applying the film theory model, the expression becomes [67]

$$\frac{R}{1 - R} = \frac{\sigma}{1 - \sigma} \left\{ 1 - \exp\left[-\frac{J_w(1 - \sigma)}{P}\right] \right\} \exp\left(-\frac{J_w}{k}\right) \quad \text{Eqn (25)}$$

Eqn (25) is the final equation for Spiegler-Kedem film theory model. The membrane characteristic parameters ( $B$ ,  $\sigma$  and  $k$ ) can be determined from experimental data of  $R$  and  $J_w$  and using the technique of non-linear regression.

**CHAPTER 3**  
**THEORY AND EXPERIMENT**

### 3. Theory and Experiment

#### 3.1. Extended Solution-Diffusion-Convection (xSDC) Model

##### 3.1.1. Water transport

The xSDC model developed by Wang et al. [68] incorporates membrane structure parameters such as porosity ( $\varepsilon$ ), membrane pore size ( $r_p$ ), membrane thickness ( $\Delta x$ ) and solute-membrane-solution interaction energy based on the classical diffusion model. Equation of the volumetric flux through the membrane can be written as

$$J_w = \frac{D_{wm} K_{wm} V_w}{RT \Delta x} (\Delta P - \Delta \pi) = A (\Delta P - \Delta \pi) = \left[ \frac{m}{s} \right] \quad \text{Eqn (26)}$$

where  $K_{wm}$  is water solubility coefficient in the membrane, which is described as

$$K_{wm} = \frac{\text{concentration of water in membrane}}{\text{concentration of water in feed}} = \frac{C_w^m}{C_w^f} \quad \text{Eqn (27)}$$

$$\begin{aligned} C_w^m &= \frac{\text{mass of water in membrane}}{\text{volume of membrane}} \\ &= \frac{\text{mass of water in membrane}}{\text{volume of membrane pore} \times \frac{1}{\text{membrane porosity}}} \\ &= C_w^p \varepsilon \end{aligned} \quad \text{Eqn (28)}$$

$$K_{wm} = \frac{C_w^p \varepsilon}{C_w^f} = \phi \cdot \varepsilon \quad \text{Eqn (29)}$$

$$D_{wm} = K_d D_\infty \quad \text{Eqn (30)}$$

where  $\phi$  represents the solution membrane partition coefficient. Combining all the equations

above (26-30) together yields

$$J_w = \frac{K_{dw} D_w^\infty \phi V_w}{RT} \frac{\varepsilon}{\Delta x} (\Delta P - \Delta \pi) \quad \text{Eqn (31)}$$

where  $K_{dw}$  is diffusion hindrance coefficient of water;  $D_\infty$  is bulk diffusion coefficient;  $\varepsilon$  is membrane porosity;  $\phi$  is solution membrane partition coefficient, which is expressed as [69]

$$\phi = 2 \int_0^{1-\lambda} g(\rho) \rho d\rho \quad \text{Eqn (32)}$$

where  $\lambda$  is radius of a molecule in the solution (*i.e.*, water molecule) over membrane pore size;  $g(\rho)$  is radial distribution function, which is expressed by the Boltzmann equation as follows [69]

$$g(\rho) = \exp\left(-\frac{\Delta G_w}{kT}\right) \quad \text{Eqn (33)}$$

Combining the solute partition model with the volumetric flux model (Eqn 26) yields

$$A = \frac{J_w}{\Delta P - \Delta \pi} = \frac{K_{dw} D_w^\infty \varepsilon V_w}{\Delta x RT} (1 - \lambda_w)^2 \exp\left(-\frac{\Delta G_w}{kT}\right) \quad \text{Eqn (34)}$$

where  $\Delta G_w$  is the water-membrane interaction energy defined below,

$$\Delta G_w = -2A_S (\sqrt{\gamma_w^{LW} \gamma_m^{LW}} + \sqrt{\gamma_w^+ \gamma_m^-} + \sqrt{\gamma_w^- \gamma_m^+}) \quad \text{Eqn (35)}$$

and  $\gamma_i^{LW}$  is the apolar (Lifshitz-van der Waals) component of the surface tension,  $\gamma_i^+$  and  $\gamma_i^-$  are the polar (electron-acceptor and electron-donor, respectively) components of the surface tension.

$A$  ( $A = \pi r_w^2/2$ ) is the contact area between a water molecule and the membrane surface.

### 3.1.2. Solute transport

In the xSDC model, the transport mechanism of solute  $J_s$  ( $\text{kg}\cdot\text{m}^{-2}\cdot\text{s}^{-1}$ ) is composed of both convection and diffusion components. The original xSDC equation is expressed as [20]

$$J_s = J_s^D + J_s^C = -K_d D_s^\infty \frac{dC}{dx} + \frac{J_w}{\varepsilon} K_c C \quad \text{Eqn (36)}$$

where  $K_d$  and  $K_c$  are diffusion hindrance and convection hindrance factors, respectively.  $C$  is the solute concentration in the membrane. The observed solute rejection can be obtained by integrating using the following boundary conditions.

$$\begin{aligned} \text{at } x = 0 : c(x = 0) &= \phi_s \beta C_f; \\ \text{at } x = \Delta x : c(x = \Delta x) &= \phi_s C_p; \end{aligned}$$

to obtain,

$$R = 1 - \frac{\beta \Phi K_c}{1 - ((1 - \Phi K_c) \exp\left(-\frac{J_w K_c \Delta x}{K_d \varepsilon D_\infty}\right))} \quad \text{Eqn (37)}$$

Bungay and Brenner proposed [70] that  $K_c$  and  $K_d$  are function of  $\lambda$  ( $\lambda = r_s/r_p$ ,  $0 < \lambda < 1$ ), which are defined as follow

$$K_c = (2 - (1 - \lambda)^2)(1 + 0.054\lambda - 0.988\lambda^2 + 0.441\lambda^3) \quad \text{Eqn (38)}$$

$$K_d = 1 - 2.3\lambda + 1.154\lambda^2 + 0.224\lambda^3 \quad \text{Eqn (39)}$$

where  $\phi$  is the solute partition coefficient that can be expressed as

$$\phi = 2 \int_0^{1-\lambda} g(\rho) \rho d\rho \quad \text{Eqn (40)}$$

$$g(\rho) = \exp\left(-\frac{\Delta G_s}{kT}\right) \quad \text{Eqn (41)}$$

where  $\Delta G_s$  is solute-membrane-solution interaction energy, which can be calculated by the Dupré equation as follows [71]

$$\Delta G_i = A\Delta G_{SLM} = 2A \left[ \sqrt{\gamma_S^{LW}\gamma_L^{LW}} + \sqrt{\gamma_M^{LW}\gamma_L^{LW}} - \sqrt{\gamma_S^{LW}\gamma_M^{LW}} - \right. \\ \left. \gamma_L^{LW} + \sqrt{\gamma_L^+}(\sqrt{\gamma_S^-} + \sqrt{\gamma_M^-} - \sqrt{\gamma_L^-}) + \sqrt{\gamma_L^-}(\sqrt{\gamma_S^+} + \sqrt{\gamma_M^+} - \right. \\ \left. \sqrt{\gamma_L^+}) - \sqrt{\gamma_S^+\gamma_M^-} - \sqrt{\gamma_S^-\gamma_M^+} \right] \quad \text{Eqn (42)}$$

The xSDC model includes both solute diffusion and convection because NF/RO membranes are not absolutely impermeable barriers as any defects on the membrane surface would induce solute convection along with water flux. The xSDC model accounts for membrane structure parameters such as membrane pore size and structure factor, which are the key elements in membrane performance. This model also includes the membrane-solution interaction energy, which reflects the degree of solute partitioning into the membrane. Therefore, the xSDC model will greatly enhance the description of the mass transfer phenomenon by incorporating energetic interactions between solute and membrane, and membrane structure parameters

### 3.1.3. General description of xSDC model

The xSDC model is visualized through Matlab<sup>®</sup> programing, which may help to understand the relationships among water permeability, solute rejection and other parameters in the model. Figure 3.1 shows that water permeability declines as water-membrane interaction energy increases. It also shows that water permeability increases as  $\lambda(r_w/r_p)$  and membrane structure factor decreases. Figure 3.2 reveals that membrane tends to show poor rejection when solute-water-membrane interaction energy is low. Comparing with  $\lambda(r_s/r_p)$ , the membrane

structure factor has less impact on solute rejection.

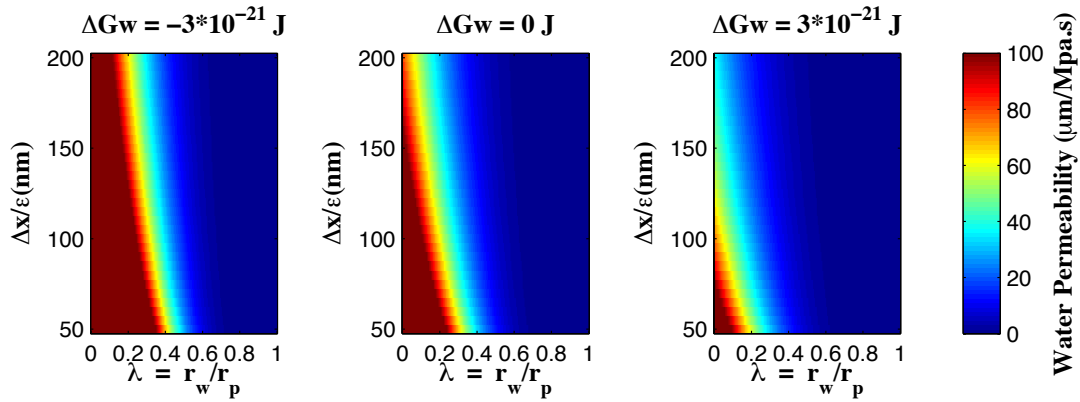


**Figure 3.1.** Combined effects of membrane structure factor, membrane pore size and water-membrane interaction energy on water permeability.

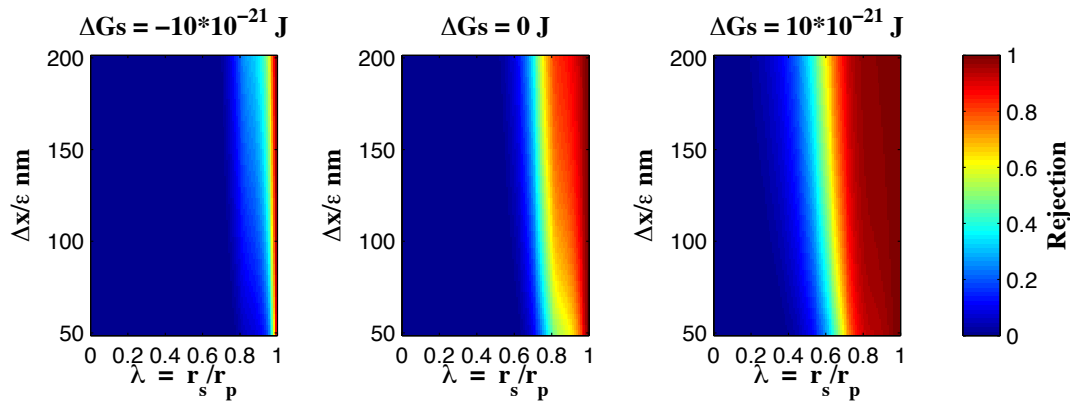


**Figure 3.2.** Combined effects of membrane structure factor, membrane pore size and solute-water-membrane interaction energy on solute rejection.

### 3.2. Membranes: NF90, NF270, and XLE

In this research three widely used membranes were evaluated: NF-90, NF-270 and low-pressure reverse osmosis (LPRO) XLE (Film Tec Corp., Minneapolis, MN). Membranes were shipped as flat sheets and all stored in deionized water (NanoPure water) at 4°C before use. According to the fact sheet provided by Film-Tec, the selective layer of NF-90 and XLE are made of polyamide, the structure of which is shown in Figure 3.3 (a). NF-270 has a semi-aromatic selective layer derived from piperazine as shown in Figure 3.3 (b). All the membranes are negatively charged above pH 3 [72]. Carvalho et al. [73] revealed that membrane surface charge under pH 7 and 30µm/cm KCl solution were -24.9, -21.6 and -3.2 mV, respectively.

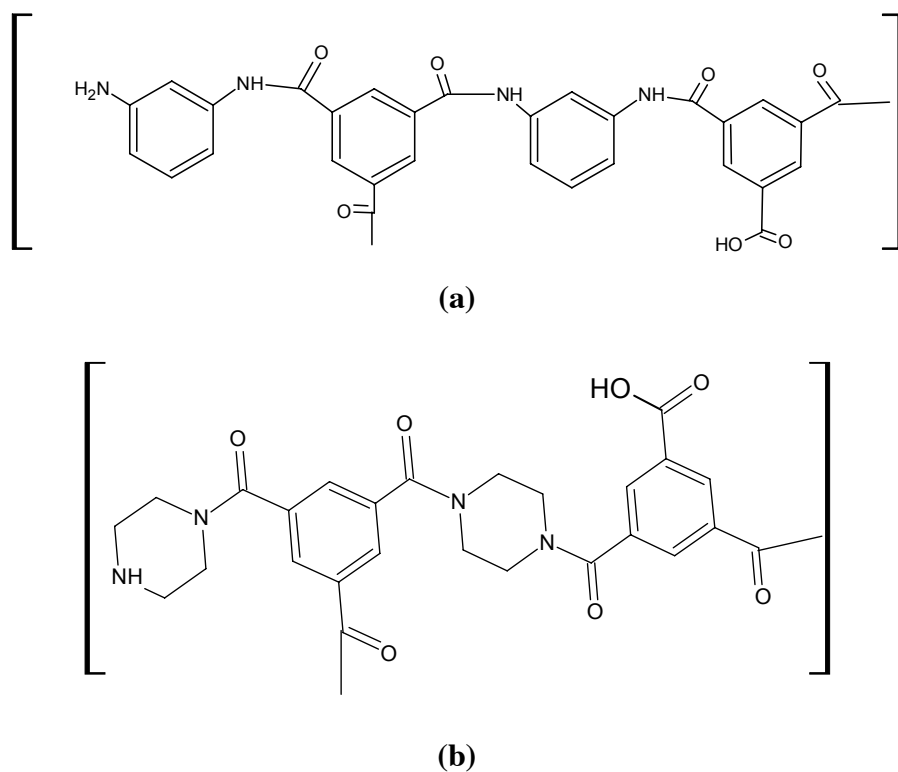


**Figure 3.3.** Chemical Structure of (a) Polyamide and (b) Poly piperazine.

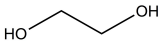
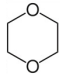


The chemical structure indicates that polyamide is fully aromatic containing benzene rings, which makes the membrane structure tighter. On the other hand, semi-aromatic piperazine has a less rigid structure than polyamide, which makes the membrane structure looser. Also, semi-aromatic piperazine adopts a chair conformation in three-dimensions, which means the inter-monomer structure is looser than polyamide. From these structural aspects, we can expect that membrane pore size for NF-90 and XLE are smaller than NF-270. Plakas et al. [74] have reported that membrane pore size of NF90, NF270, and XLE obtained from Atomic Force Microscopy (AFM) were  $0.55\pm 0.13$ ,  $0.71\pm 0.14$  and  $0.67$  nm, respectively. The NaCl retentions were 99.5%, 66.4% and 95.9%, respectively [74]. Hence, membrane pore size and membrane surface charge have great impact on salt rejection.

### **3.3. Solutes: Ethylene Glycol and 1,4-dioxane**

Ethylene Glycol (EG) and 1,4-dioxane were the solutes chosen for rejection testing. Physical-chemical properties of EG and 1,4-dioxane are shown in Table 3.1. EG is a short chain compound with a stokes radius of 0.183 nm. It is neutral organic molecule in water because of its high pKa. 1,4-Dioxane is a ring compound with a stokes radius is 0.23 nm. It is also an uncharged organic molecule due to no dissociable functional group. Thus, these two compounds are good candidates for uncharged solutes for the rejection test.

**Table 3.1.** Physic-chemical properties of EG and 1,4-dioxane.

Organics	Molecular Weight (g/mol)	Molecular Structure	Stokes radius <sup>a</sup> (nm)	Diffusivity <sup>[47]</sup> (cm <sup>2</sup> /s)	pK <sub>a</sub>	pK <sub>ow</sub>
EG	62.07		0.183	1.16×10 <sup>-5</sup>	14.2 <sup>[75]</sup>	1.36 <sup>[76]</sup>
1,4-dioxane	88.11		0.23	0.97×10 <sup>-5</sup>	-2.92 <sup>[77]</sup>	-0.27 <sup>[77]</sup>

Stokes radius was calculated according to classical stokes equation

### 3.4. Water chemistry: Concentration, pH, Divalent ions

Three different categories of water chemistry were used to evaluate all solutions tested: concentration of solutes, pH of solution, and composition of divalent ions. Concentrations of 5mM, 50mM, and 500mM of NaCl solutions were tested in order to represent fresh water, brackish water and seawater, respectively. pH were adjusted ranging from 3 to 11 to cover the optimal operating pH range for polyamide membranes. Ca<sup>2+</sup> and Mg<sup>2+</sup> are the common ions chosen in the water to demonstrate the effect of divalent ions. The ionic strength for pH and divalent sections were maintained around 50mM NaCl. The temperature of the feed solution was maintained constant at 20°C under stirring using a chiller (Thermo Fisher, Hampton, NH).

### 3.5. Analytic method

Conductivity and pH of feed and permeate water were measured using a calibrated pH and conductivity meter (Thermo Fisher). Water volumetric flux (ml/min) was recorded three times at each pressure by GJC flow meter (London). Permeate samples were all measured for

non-purgeable organic carbon (NPOC) by using TOC (Shimadzu). TOC taken to be the average of three measured values.

### 3.6. Contact angle measurements

Three membranes were rinsed with DI water and stored in a desiccator for 3 days before use. The instrument for contact angle was bought from KRÜSS (Germany). Two polar solutions and one apolar solution were titrated on each membrane. DI water under ten chemistries was used as polar liquid and the other two liquids were diiodomethane (apolar) and Glycerol (polar). At least fifteen equilibrium contact angles were measured for each membrane. The highest and lowest values were discarded before taking the average contact angle.

### 3.7. Membrane surface tension parameters

Membrane surface tension parameters in ten different water chemistries can be calculated using the Young-Dupre equation [71].

$$(1 + \cos\theta)\gamma_L = 2 \left( \sqrt{\gamma_M^{LW}} \sqrt{\gamma_L^{LW}} + \sqrt{\gamma_M^+} \sqrt{\gamma_L^-} + \sqrt{\gamma_M^-} \sqrt{\gamma_L^+} \right) \quad \text{Eqn (43)}$$

where  $\theta$  is contact angle between solution and membrane,  $\gamma_i^{LW}$  is the apolar (Lifshitz-van der Waals) component of the surface tension, which represents organic part of membrane;  $\gamma_i^+$  and  $\gamma_i^-$  are the polar (electron-acceptor and electron-donor) components of the surface tension, which represent hydrophobic part and hydrophilic part, respectively. The apolar and polar data for solution can be acquired from previous literature. Based on Eqn (43), three contact angles of known solution can determine the surface tension parameters of one membrane, and vice versa.

### **3.8. Performance testing**

Six pieces of membrane were used at each time, and each membrane has two replicates. Membranes were all compacted at 450 psi for 16 hours with recirculating DI water. Membrane flux was measured and ensured it was stable (membrane compacted) before proceeding. Organic solute was added into feed water tank after adjusting water chemistry. Then, the system was run 12 hours at 280 psi to reach to equilibrium in order to eliminate the effect of adsorption on the membrane matrix as a variable. Permeate were collected at five different applied pressures. pH and conductivity were measured immediately. Samples were all stored at 4°C before measuring TOC. The filtration system was washed three times with tap-DI water after experiment. Water permeability was measured after cleaning, and if the water permeability had less than 10% variation from the previous measurement, the same membrane was used for another organic rejection experiment under same water chemistry.

**CHAPTER 4**  
**RESULT AND DISCUSSION**

## 4. Results and Discussions

### 4.1. Membrane characterization

The contact angles of DI-water, Diiodomethane and EG with three membranes are listed in Table 4.1. NF90 and XLE have similar contact angles, which imply that they may have similar membrane performance. NF270 has low contact angle with DI-Water, indicating high affinity to water, which may reflect higher water permeability than NF90 and XLE. Surface tension components of three solutions are listed in Table 4.2. Membrane surface tension components are shown in Table 4.3.

**Table 4.1.** Contact angle of membranes with Water, Diiodomethane and EG.

	Contact Angle (°)		
	DI-Water	Diiodomethane	EG
NF90	69.89±1.61	35.93±1.06	25.08±1.27
NF270	28.25±1.59	38.73±1.95	12.55±1.35
XLE	70.12±1.80	38.16±0.75	26.68±1.44

**Table 4.2.** Surface tension parameters of solutes.

Chemicals	$\gamma_S^T$ (mJ/m <sup>2</sup> )	$\gamma_S^{LW}$ (mJ/m <sup>2</sup> )	$\gamma_S^+$ (mJ/m <sup>2</sup> )	$\gamma_S^-$ (mJ/m <sup>2</sup> )
EG	48	29	1.92	47
Diiodomethane	50.8	50.8	0	0
Water	72.8	26.22	25.5	25.5

**Table 4.3.** Membrane surface tension parameters in ten water chemistries.

Solutions	Contact	$\gamma_M^{LW}$	$\gamma_M^+$	$\gamma_M^-$	$\gamma_M^{AB}$	$\Delta G_{SL}$	$\Delta G_{SLs}$	
	Angle (°)	(mJ/m <sup>2</sup> )	(mJ/m <sup>2</sup> )	(mJ/m <sup>2</sup> )	(mJ/m <sup>2</sup> )	(mJ/m <sup>2</sup> )	(mJ/m <sup>2</sup> )	
NF90	DI Water	69.89±1.61	41.64	1.14	7.027	5.66	-97.81	-44.57
	NaCl 5 mM	65.52±1.51	41.64	0.88	10.82	6.17	-102.95	-35.32
	NaCl 50 mM	62.97±1.20	41.64	0.75	13.33	6.32	-105.87	-29.78
	NaCl 500 mM	61.00±1.39	41.64	0.66	15.41	6.36	-108.08	-25.43
	NaCl 50 mM,pH=3	67.66±2.54	41.64	1.00	8.88	5.97	-100.46	-39.89
	NaCl 50 mM,pH=5	64.67±0.91	41.64	0.83	11.64	6.23	-103.94	-33.46
	NaCl 50 mM,pH=7	62.19±1.31	41.64	0.71	14.14	6.34	-106.75	-28.06
	NaCl 50 mM,pH=9	60.93±1.39	41.64	0.65	15.48	6.36	-108.15	-25.29
	NaCl 50 mM,pH=11	56.26±1.89	41.64	0.46	20.82	6.21	-113.22	-14.87
	MgCl <sub>2</sub> 50 mM	61.44±1.47	41.64	0.68	14.93	6.35	-107.58	-26.42
CaCl <sub>2</sub> 50 mM	64.04±1.53	41.64	0.80	12.26	6.27	-104.67	-32.09	
NF270	DI Water	28.25±1.59	40.29	0.22	52.04	6.84	-136.91	33.98
	NaCl 5 mM	30.96±1.62	40.29	0.27	49.04	7.23	-135.21	29.78
	NaCl 50 mM	26.38±1.99	40.29	0.20	54.01	6.56	-138.01	36.70
	NaCl 500 mM	22.80±3.51	40.29	0.16	57.51	6.05	-139.89	41.50
	NaCl 50 mM,pH=3	27.47±2.38	40.29	0.21	52.87	6.72	-137.38	35.13
	NaCl 50 mM,pH=5	24.46±0.58	40.29	0.18	55.94	6.29	-139.05	39.36
	NaCl 50 mM,pH=7	23.91±1.22	40.29	0.17	56.46	6.21	-139.33	40.07
	NaCl 50 mM,pH=9	20.04±1.34	40.29	0.13	59.94	5.68	-141.17	44.80
	NaCl 50 mM,pH=11	17.15±1.63	40.29	0.11	62.21	5.33	-142.34	47.85
	MgCl <sub>2</sub> 50 mM	21.13±1.92	40.29	0.14	59.03	5.82	-140.70	43.56
CaCl <sub>2</sub> 50 mM	25.71±1.77	40.29	0.19	54.69	6.47	-138.38	37.64	
XLE	DI Water	70.12±1.80	40.53	1.18	7.22	5.83	-97.54	-43.23
	NaCl 5 mM	70.03±2.38	40.53	1.17	7.29	5.84	-97.65	-43.05
	NaCl 50 mM	67.83±2.55	40.53	1.03	9.14	6.15	-100.26	-38.44
	NaCl 500 mM	67.03±2.19	40.53	0.99	9.86	6.24	-101.20	-36.74
	NaCl 50 mM,pH=3	69.85±2.47	40.53	1.16	7.44	5.87	-97.87	-42.67
	NaCl 50 mM,pH=5	66.94±0.77	40.53	0.98	9.95	6.25	-101.31	-36.54
	NaCl 50 mM,pH=7	62.96±1.84	40.53	0.77	13.86	6.52	-105.89	-27.92
	NaCl 50 mM,pH=9	61.92±1.77	40.53	0.72	14.96	6.55	-107.06	-25.63
	NaCl 50 mM,pH=11	60.34±1.96	40.53	0.64	16.69	6.55	-108.81	-22.15
	MgCl <sub>2</sub> 50 mM	65.47±2.08	40.53	0.90	11.32	6.38	-103.00	-33.41
CaCl <sub>2</sub> 50 mM	67.00±2.22	40.53	0.98	9.89	6.24	-101.24	-36.67	

The free energy of interaction between a solution and a surface is represented by  $\Delta G_{SL}$ . The value of  $\Delta G_{SL}$  indicates the hydrophilicity of membrane. The more negative value of  $\Delta G_{SL}$ , the

more hydrophilic the membrane or the higher affinity for water and vice versa.  $\Delta G_{SLS}$  refers to the free energy of cohesion of liquid between two identical surfaces. When  $\Delta G_{SLS} < 0$ , the cohesion between two surfaces is strong; when  $\Delta G_{SLS} > 0$ , the cohesion between two surfaces is weak.  $\Delta G_{SLS}$  also refers to the degree of repulsion and attraction. The more positive the value of  $\Delta G_{SLS}$ , the greater the repulsive force between polymer chains. Table 4.3 shows that membrane becomes more hydrophilic with increasing NaCl concentration, pH and the presence of  $MgCl_2$  and  $CaCl_2$ . The trend of  $\Delta G_{SLS}$  data shows repulsive force increased as salinity and pH increased. An explanation to describe this phenomenon is to consider polymer swelling under different water chemistries. The data suggests that the polymeric membrane swells under higher salinity and higher pH waters shown in an increase of repulsive force between polymer chains in the membrane ( $\Delta G_{SLS}$ ).

#### **4.2. Solute-membrane-solution interaction energy**

The interaction energy of membrane-EG-water and membrane-water were calculated according to Dupré equation, results are listed in Table 4.4. The interaction energy  $\Delta G_s$  can be considered as the quantification of attractive or repulsive solute-membrane-solution affinity interaction [20]. When  $\Delta G_s$  is positive, the membrane repels the solute, which means it is not easy for solute to diffuse into membrane matrix. Verliefde et al. [20] reported that solute partition coefficient will be low when  $\Delta G_s > 0$ . Table 4.4 showed that  $\Delta G_s$  of NF270 were more positive than NF90 and XLE, which means NF270 has larger repulsion force to EG than NF90 and XLE. Because EG is a moderate hydrophobic solute, so NF270 is more hydrophilic than NF90 and



XLE. It is noteworthy that all  $\Delta G_w$  were negative for three membranes, it means there is an attraction force between membrane and water. Beside, we noticed that  $\Delta G_w$  of NF270 were more negative than NF90 and XLE, which also indicates that NF270 is more hydrophilic than NF90 and XLE.

**Table 4.4.** Interaction energy of membrane-solute-water and membrane-water for EG.

Solutions	NF90		NF270		XLE	
	$\Delta G_s$ $10^{-21}\text{J}$	$\Delta G_w$ $10^{-21}\text{J}$	$\Delta G_s$ $10^{-21}\text{J}$	$\Delta G_w$ $10^{-21}\text{J}$	$\Delta G_s$ $10^{-21}\text{J}$	$\Delta G_w$ $10^{-21}\text{J}$
NaCl 5 mM	-0.03	-1.96	1.33	-2.57	-0.25	-1.85
NaCl 50 mM	0.11	-2.01	1.46	-2.62	-0.13	-1.90
NaCl 500 mM	0.21	-2.05	1.55	-2.66	-0.08	-1.92
NaCl 50 mM,pH=3	-0.15	-1.91	1.43	-2.61	-0.24	-1.86
NaCl 50 mM,pH=5	0.02	-1.97	1.51	-2.64	-0.08	-1.92
NaCl 50 mM,pH=7	0.15	-2.03	1.52	-2.65	0.14	-2.01
NaCl 50 mM,pH=9	0.22	-2.05	1.61	-2.68	0.19	-2.03
NaCl 50 mM,pH=11	0.45	-2.15	1.66	-2.70	0.27	-2.07
MgCl <sub>2</sub> 50 mM	0.19	-2.04	1.59	-2.67	0.00	-1.96
CaCl <sub>2</sub> 50 mM	0.05	-1.99	1.48	-2.63	-0.08	-1.92

### 4.3. Performance test results for EG

#### 4.3.1. Effect of water chemistry on membrane water permeability

##### 4.3.1.1. Effect of ionic strength

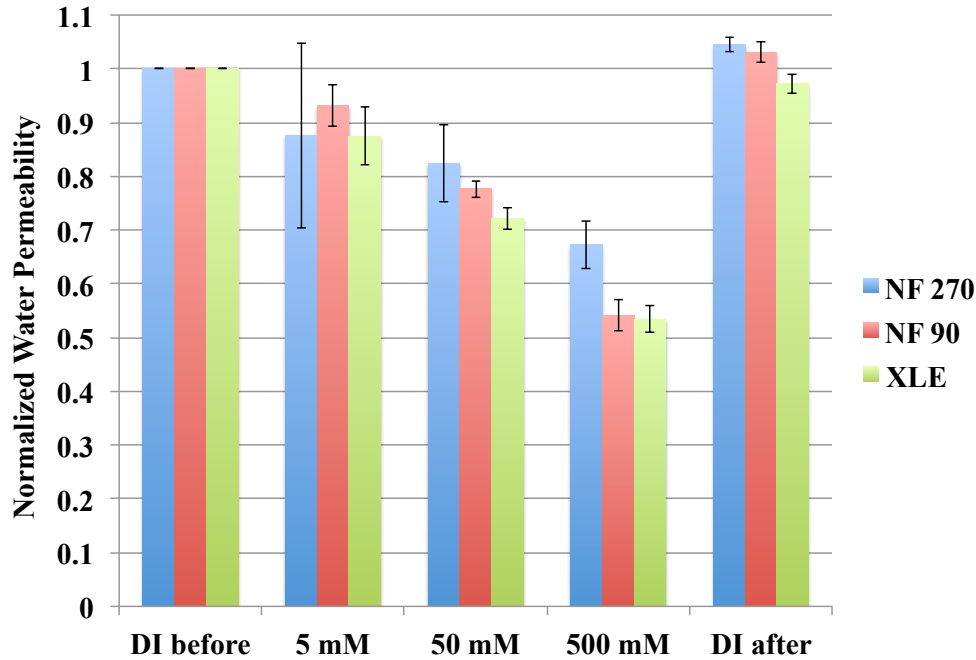


**Figure 4.1.** Effect of ionic strength (NaCl) on membrane water permeability.

Membrane water permeability was evaluated while changing the ionic strength of feed water. As shown in Figure 4.1, for all the membranes, membrane water permeability decreased as ionic strength in the feed water increased. Among the three commercial membranes, the loss of water permeability for NF270 (up to 33 %) was less significant compared to NF90 and XLE (up to 47 %). XLE, which is the least permeable membrane in this study, suffered the highest loss in water permeability (up to 47 %) under feed water with high ionic strength. For all the three membranes, water permeability was almost fully recovered when filtered pure water through,

indicating that dissolved ionic compounds, even at high ionic strengths, do not cause irreversible changes to the membrane

#### 4.3.1.2. Effect of pH

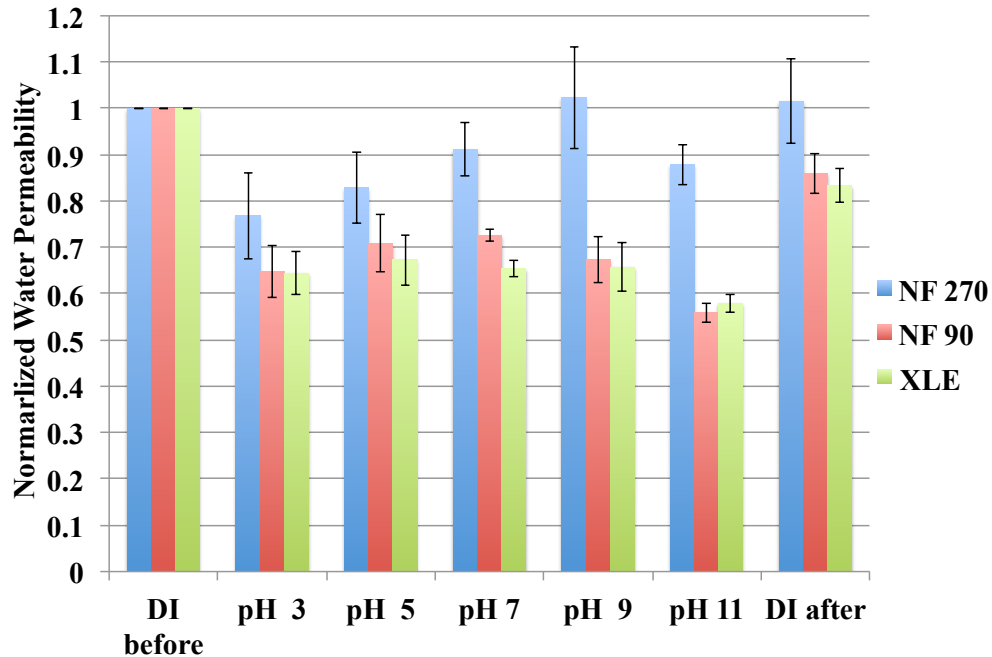


**Figure 4.2.** Effect of pH on membrane water permeability.

Effect of pH on membrane water permeability was also studied in this work as presented in Figure 4.2. For NF270, when pH was increased from 3 to 9, membrane water permeability also increased. When feed water pH was further increased to 11, membrane water permeability dropped. For NF90 and XLE, when pH was raised from 3 to 7, membrane water permeability increased. When feed water pH further increased from 7 to 11, membrane water permeability dropped. However, water permeability of NF90 and XLE were less sensitive to solution pH than

NF270. Pure water permeability of NF270 could be completely recovered, while the changes in NF90 and XLE pure water permeability were less reversible. The irreversibility may be attributed to the difference in chemical composition in polyamide versus polypiperazamide

#### 4.3.1.3. Effect of divalent ions

Divalent ions (*i.e.*,  $\text{Ca}^{2+}$ ,  $\text{Mg}^{2+}$ ) are widely distributed in natural fresh and wastewater and they have the importance to be studied. As shown in Figure 4.3, for all the membranes, water permeability was lower when  $\text{Ca}^{2+}$  or  $\text{Mg}^{2+}$  was present in the feed compared to pure water as the feed. Furthermore, the loss of water permeability (30 – 40 %) was more than that when the same concentration of NaCl was used as the feed (20 – 30 %). There was no significant difference in the reduction percentage of water permeability among three tested membranes. However, the membrane water permeability under 50 mM  $\text{MgCl}_2$  feed solution was lower than membrane water permeability under 50 mM  $\text{CaCl}_2$  feed for all membranes. It is interesting to point out that the pure water permeability could not be fully recovered for NF90 and XLE membranes (80 – 95 %), which may be attributed to the fully aromatic structure of the polymer chains. Based on the results, magnesium ion appeared to cause more water permeability loss for all membranes than calcium ion at the same concentration. One possible reason for these observations is the ability for the smaller  $\text{Mg}^{2+}$  (86pm) compared to the larger  $\text{Ca}^{2+}$  (114pm) to penetrate and neutralize the charge on the negatively charged polymer chains, which causes the chains to collapse and reduces free volume left for water diffusion in the membrane, thereby reducing observed water permeability.

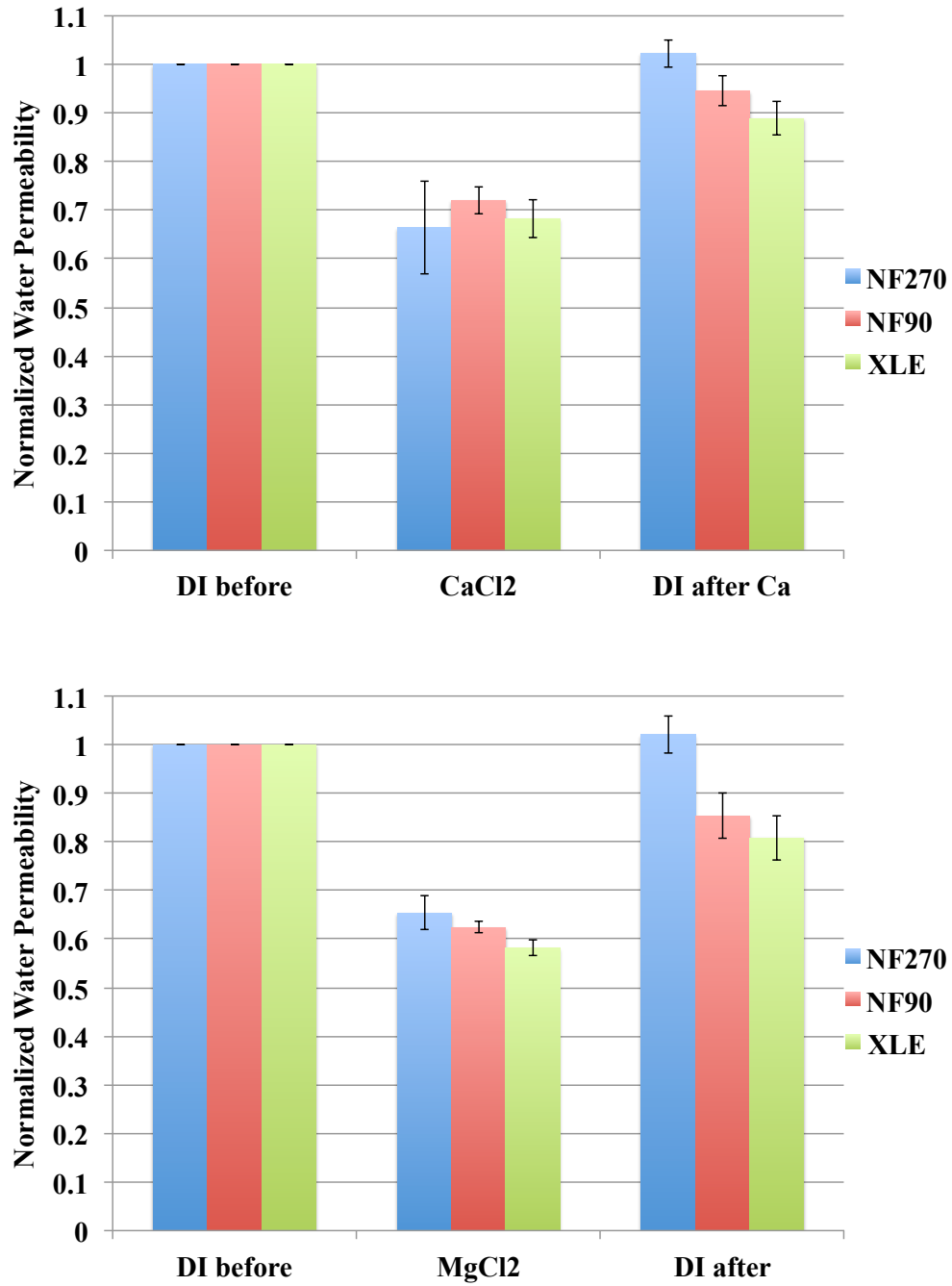
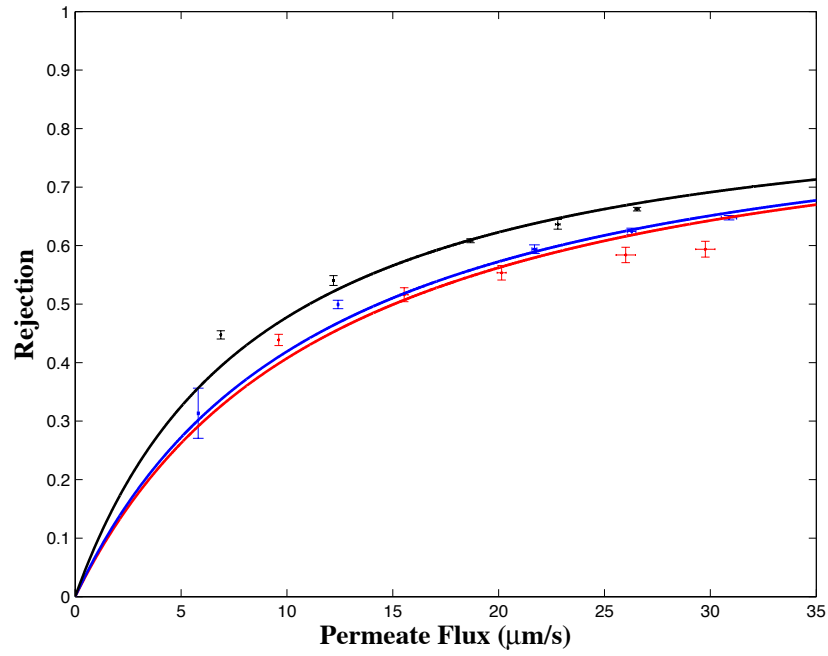


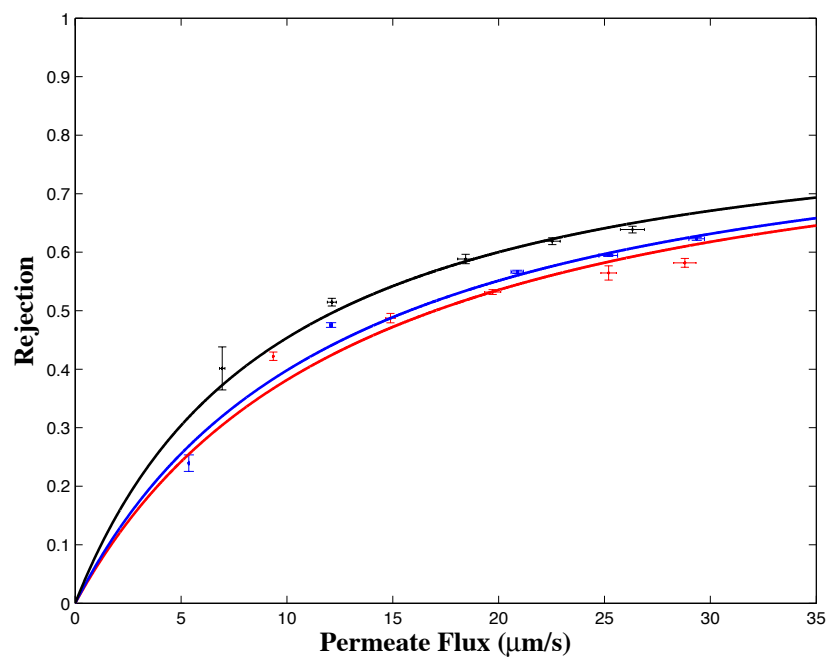
**Figure 4.3.** Effect of divalent ions on membrane water permeability.

## 4.3.2. Effect of water chemistry on EG rejection

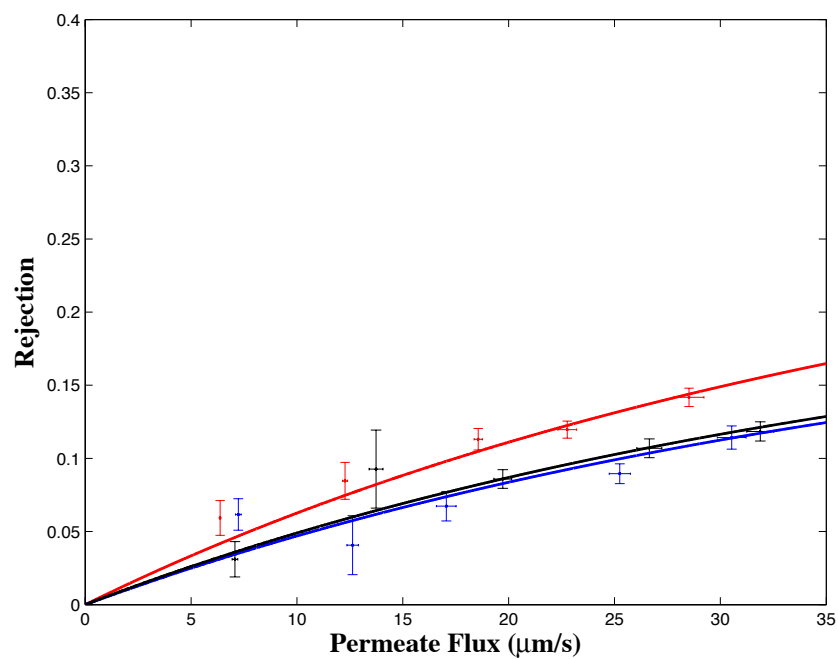
### 4.3.2.1. Effect of ionic strength



(a)



(b)



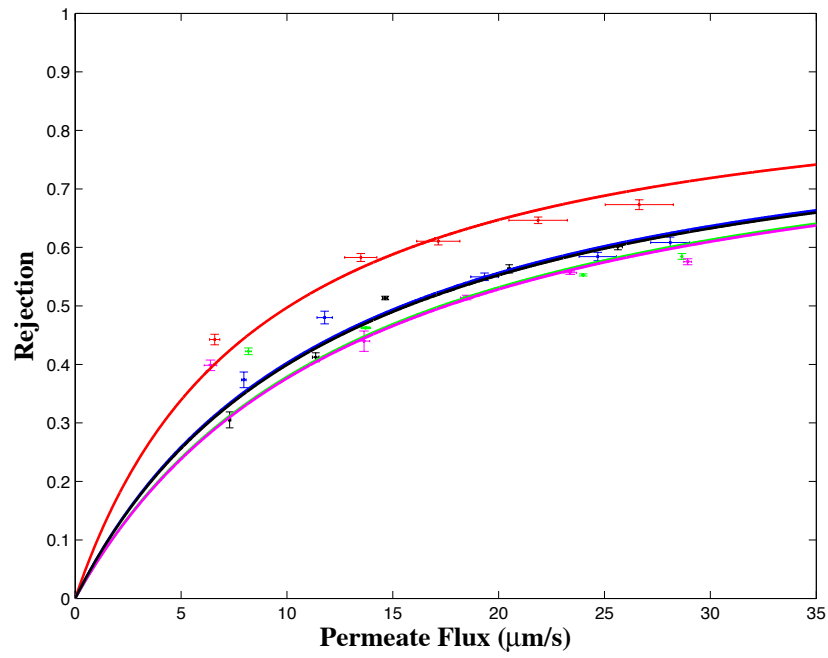
(c)

**Figure 4.4.** Effect of ionic strength (NaCl) on EG rejection for NF90 (a), XLE (b), NF270 (c) membranes (5 mM=red, 50 mM=blue, 500 mM=black).

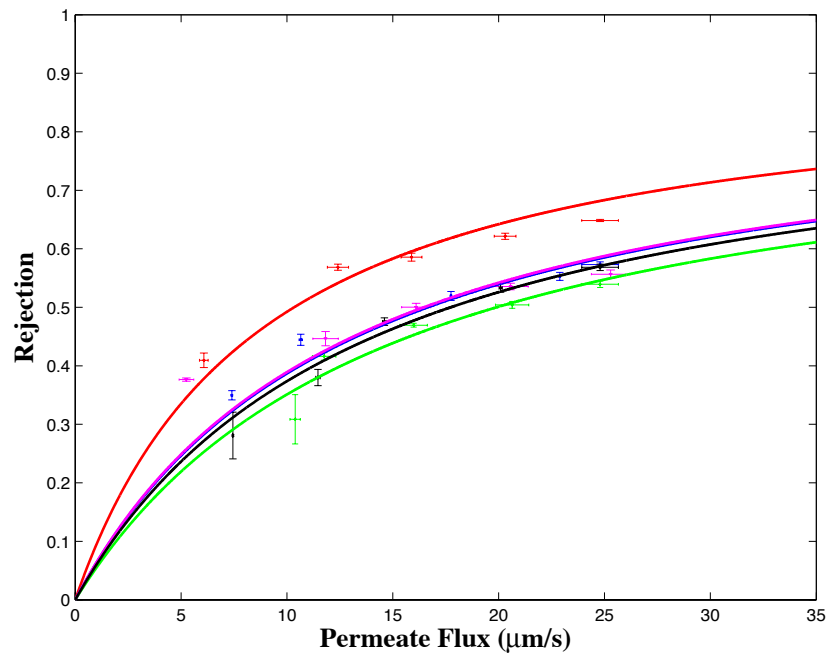
The rejection of EG by NF90 and XLE increased as ionic strength increased as shown in Figure 4.4. There was a minimal difference observed in rejection between 5 mM and 50 mM, while a 7% increase in rejection was observed from 50 mM to 500 mM. This indicates that the membrane became more selective when subjected to 500 mM NaCl. NF270 showed the opposite trends of NF90 and XLE; that is, EG rejection decreased as ionic strength increased. As the membrane pore size and the structure factor are determining elements in membrane performance, it is reasonable to expect that membrane pore size or structure factor changes as salinity increased as described previously. According to the discussion of  $\Delta G_{SLS}$  in the membrane characterization section, it is expected that NF270 will be looser as salinity increases. Details will be discussed in Section 4.5.



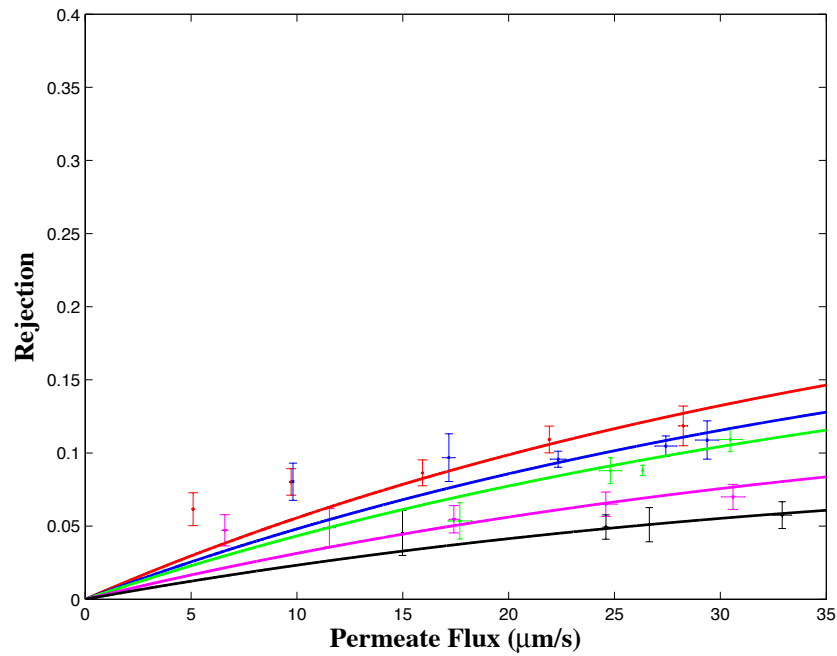
### 4.3.2.2. Effect of pH



(a)



(b)

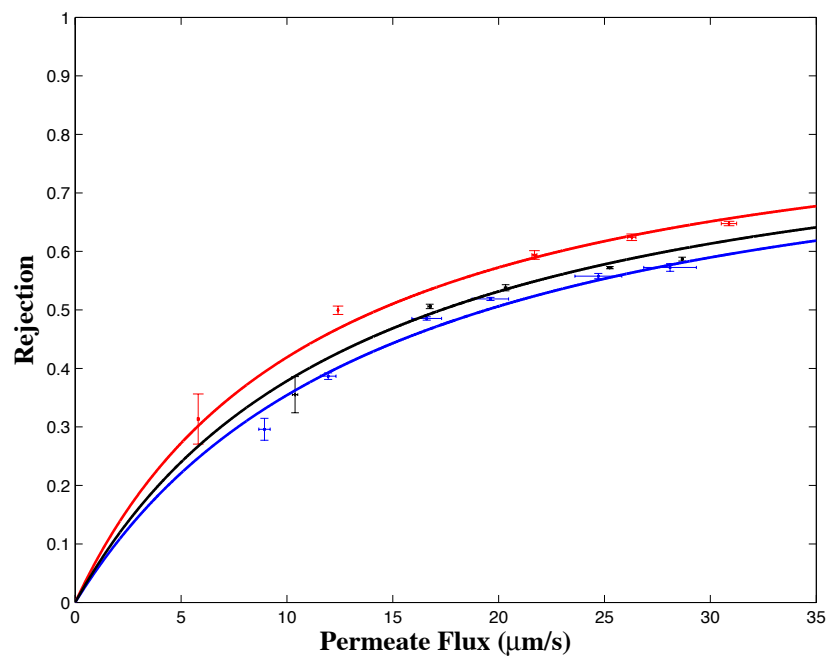


(c)

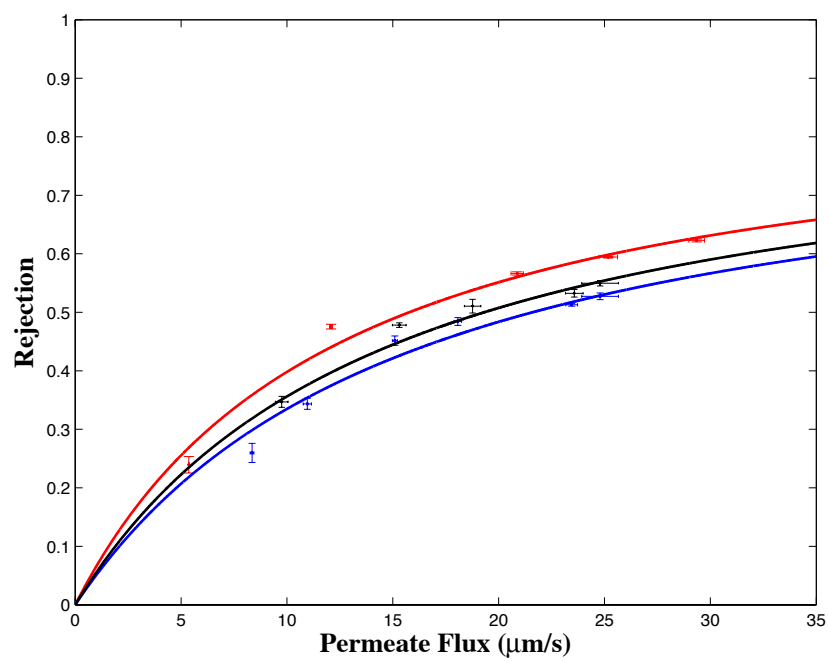
**Figure 4.5.** Effect of pH on EG rejection for NF90 (a), XLE (b), NF270 (c) membrane (pH3=red, pH5=blue, pH7=green, pH9=pink, pH11=black).

As shown in Figure 4.5, rejection of EG decreased as pH increased from 3 to 11. Rejection curves of EG were similar at pH 5, 7, 9, 11, and about 7% higher at pH 3 than at pH 5, 7, 9, 11 for XLE and NF90. NF270 also showed that EG rejection decreased as pH increased. Hence, pore size and structure factor would be smaller at pH=3 than other pH values.

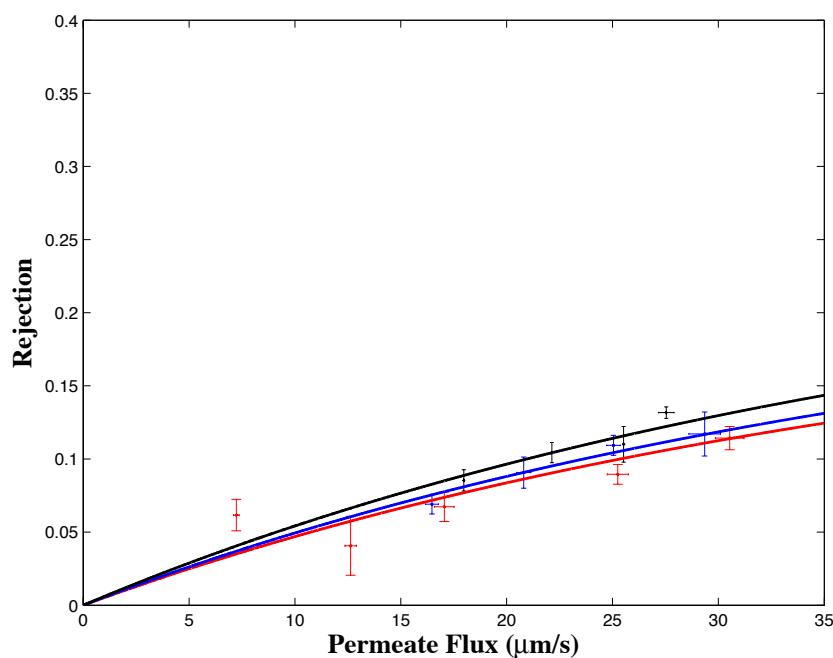
### 4.3.2.3. Effect of Divalent ions



(a)



(b)



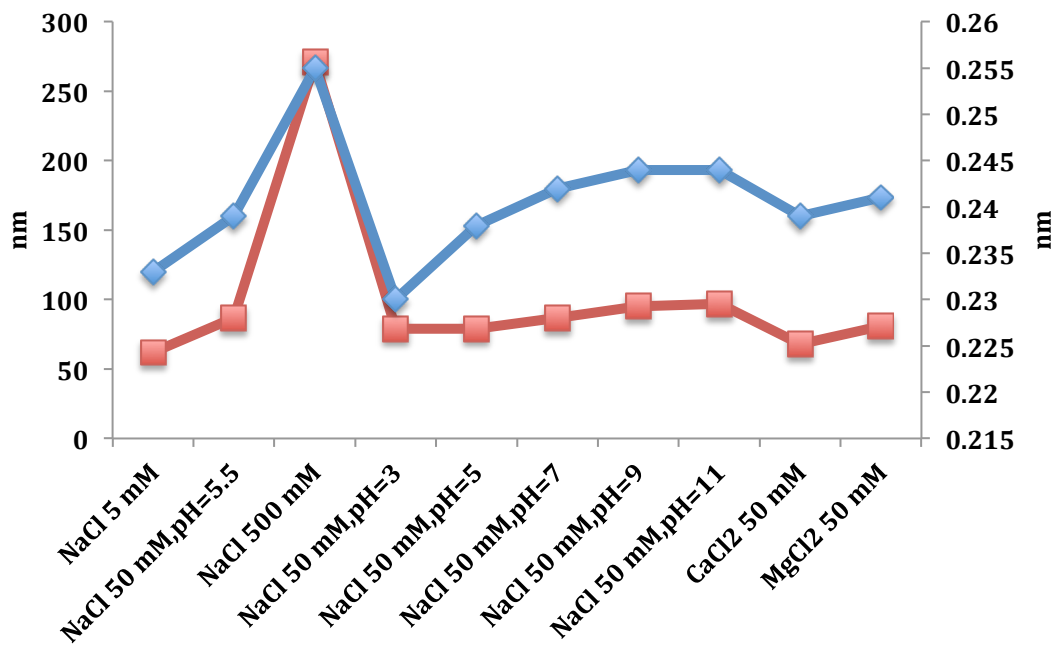
(c)

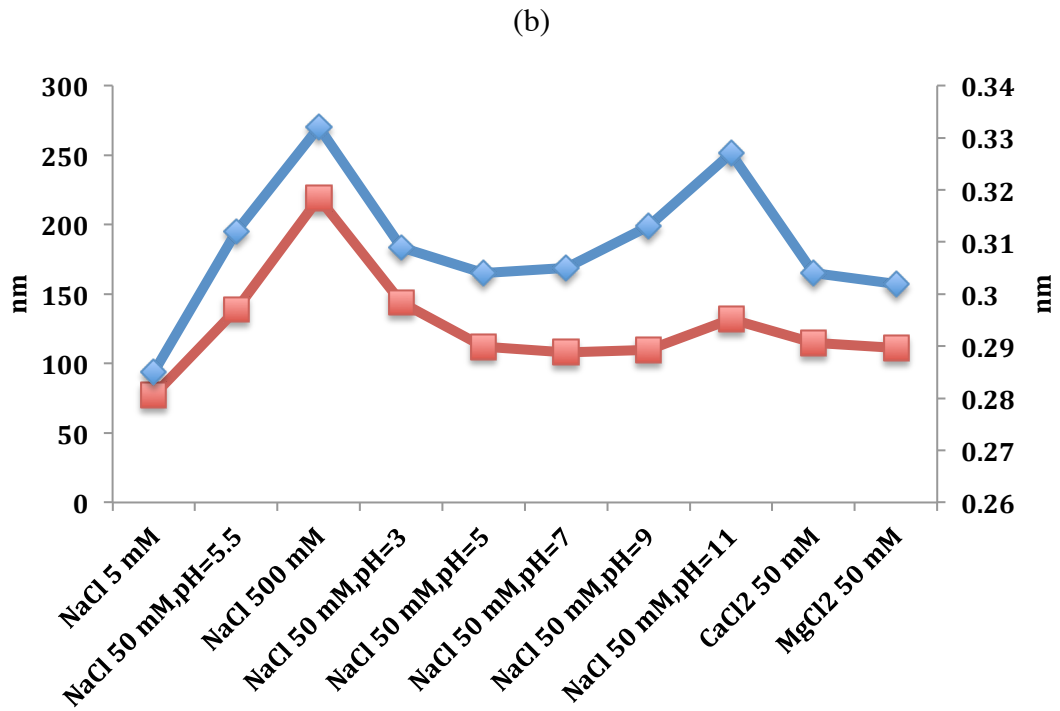
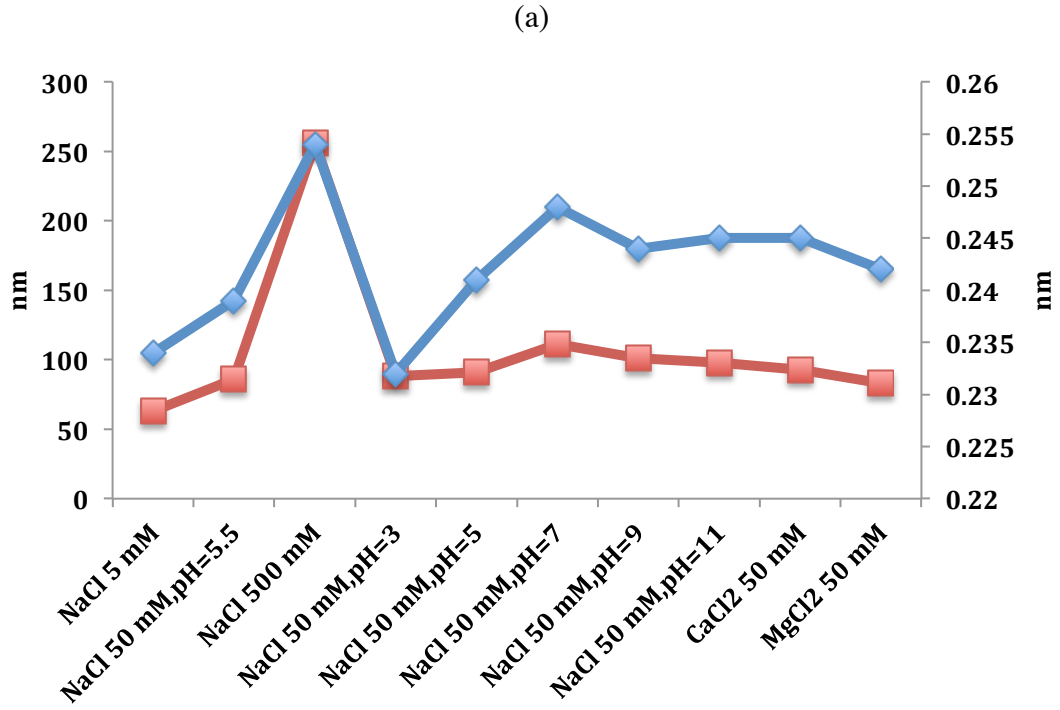
**Figure 4.6.** Effect of divalent ions ( $\text{Mg}^{2+}$ ,  $\text{Ca}^{2+}$ ) on EG rejection for NF90 (a), XLE (b), and NF270 (c) membrane (50 mM NaCl=red, 50 mM  $\text{CaCl}_2$ =blue, 50 mM  $\text{MgCl}_2$ =black).

Rejection curves for  $\text{CaCl}_2$  and  $\text{MgCl}_2$  were quite similar, which were lower than NaCl at same ionic strength for NF90 and XLE (Figure 4.6 a and b). NF270 did not perform the same trend as NF90 and XLE.  $\Delta G_{SLS}$  in Table 4.3 tells that the inter-polymers repulsive force in divalent ions is greater than in  $\text{Na}^+$  at same ionic strength for the three membranes, except for NF90 in  $\text{CaCl}_2$  50 mM. It would be consistent to saying that membrane pore size and structure factor are larger in a solution of divalent ions than in a solution of monovalent ions at the same concentration.

#### 4.4. Membrane structural parameters obtained from EG

Membrane pore size and structure factor are shown in Table 4.5. The best fitting membrane pore size and membrane structure factor can be calculated mathematically corresponding to overall rejection curves, which may help to understand the discrepancy between rejection curves for each membrane. Membrane pore sizes and structure factors of NF90, NF270, and XLE all increase as ionic strength increase from 5 mM to 500 mM and pH increased from 3 to 11. The observed phenomenon in pore size and membrane structure factor is consistent with reasonable expectations in the previous section that as salinity and pH increased, the repulsive force between polymers increased, thus resulting larger pore size and looser structure factor. The following discussions will be focusing on water permeability, overall rejection, membrane pore size, and structure factor in the three water chemistry categories.





(c)

**Figure 4.7.** Calculated membrane pore size (right blue) and structural factor (left, red) for NF90 (a), XLE (b), and NF270 (c).

First, increasing membrane pore size will result in an increase in the membrane structure factor ( $\Delta x/\varepsilon$ ), essentially causing the membrane to swell. The variability of solute rejection and water permeability can be explained from the changes in membrane structure. As shown in the fitting results, the pore size and structure factor of NF90 and XLE at 5 mM and 50 mM were similar. When ionic strength increased from 50 mM to 500 mM, the pore size increased from 0.221 nm to 0.237 nm and 0.219 nm to 0.234 nm for NF90 and XLE, respectively. Structure factor increased from 69 nm to 228 nm, 60 nm to 185 nm for NF90 and XLE, respectively. Membrane structure swelling was caused by inter-polymer repulsive forces, which increased from 5 mM to 500 mM. According to Section 3.1.3, large pore size results in poor EG rejection and thick structure factor results in low water permeability. The overall effect of pore size and structure factor is determined by the conjugated effect. Braghetta et al. [78] offered a widely accepted explanation for water permeability decline, which is that the membrane will be compressed at high ionic strength. Porosity of the membrane will be reduced due to the decrease of electrostatic charge repulsion between the negatively charge polymer chains, which is consistent with the fitting data that structure factor increased three folds from 50 mM to 500 mM. EG rejection increased as ionic strength increased due to membrane compaction. Braghetta also have observed that rejection of organic enhanced as ionic strength increased. The enhanced EG rejection also may because of increased partition coefficient [79], which means membrane becomes more hydrophilic and hydrogen bonds between solute and polymer are more easy to be formed due to loss of electrostatic interactions.

The influence of pH on organic rejection is related to membrane surface charge and

membrane structure. Membrane surface charge will increase as pH increase due to the dissociation of carboxylic group. Table 4.5 shows out that membrane pore sizes and structure increased as pH increased, which is consistent with the  $\Delta G_{SLS}$  values. The overall rejection of EG decreased as pH decreased from 3 to 11, which may be due to an increase in pore size. Bellona et al. [80] reported that the phenomenon of increasing membrane pore size as pH increases is because of the increase in repulsion forces within the membrane caused by dissociation of acidic functional groups. Water permeability increased from pH=3 to pH=7, then decreased from pH=9 to pH=11. This causes a tradeoff between an increase in membrane pore size and a decrease in membrane structure factor. Pore size and structure factor have contradictory effects on water permeability. However, Manttari et al. [81] showed that water permeability increased as pH increased, which is not consistent with observations shown in this study. An alternative reason could be membrane fouling or defective pieces of membrane.

Figure 4.7 revealed that membrane pore size under solutions containing divalent cations were larger than in NaCl. The structure factor of  $\text{Ca}^{2+}$  and  $\text{Mg}^{2+}$  were both lower than  $\text{Na}^+$  under the same ionic strength. EG rejection decreased in the presence of  $\text{Ca}^{2+}$  and  $\text{Mg}^{2+}$ , which indicated that membrane pore size might have increased. The presence of divalent ions like  $\text{Ca}^{2+}$  and  $\text{Mg}^{2+}$  will neutralize membrane surface charge [78, 80, 82] more effectively than  $\text{Na}^+$ . Especially at high concentrations of  $\text{Ca}^{2+}$  and  $\text{Mg}^{2+}$ , membrane surface charge could be positively charged, thus resulting in an increase in membrane pore.  $\Delta G_{SLS}$  value also showed that membrane pore size should increase to be consistent with the trend. No data is currently



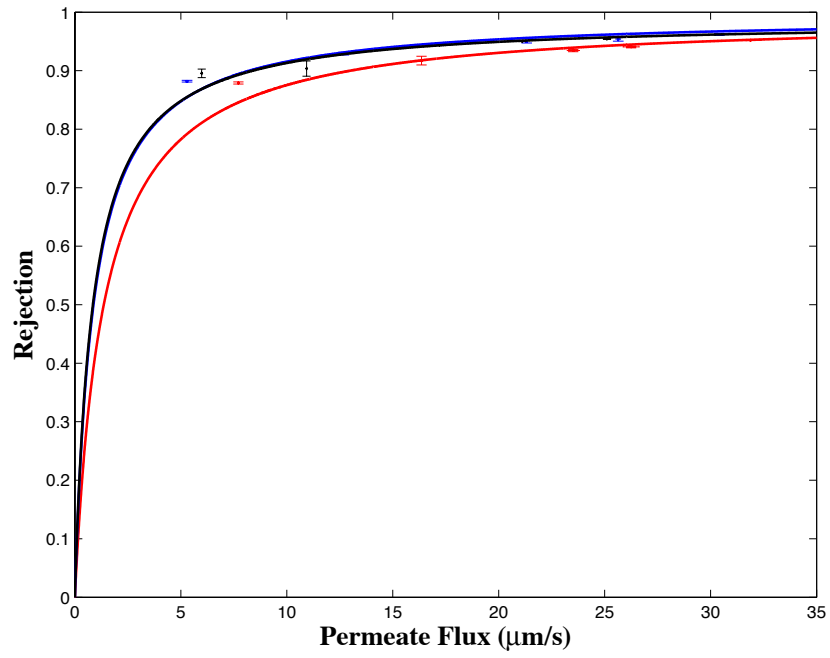
available to show the surface charge of membrane under 50 mM divalent solution, but it is still a reasonable hypothesis and more research is needed to be done to validate these explanations.

#### **4.5. Real rejection and fitting results for 1,4-dioxane**

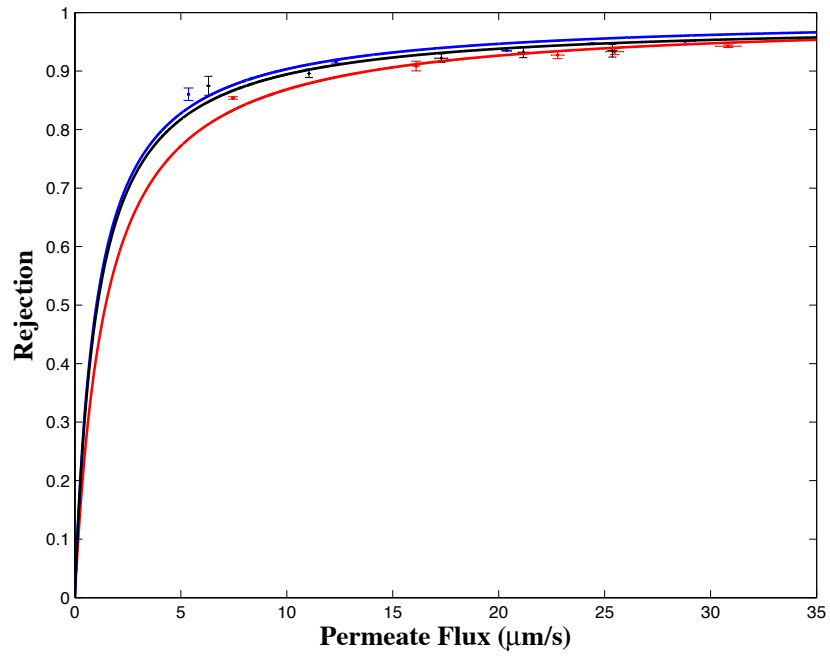
1,4-dioxane rejection experiments were carried out right after EG experiment for the same membrane and water chemistry. Since membrane structure is only affected by water chemistry, but not trace organic solute, the model fitting structural data of EG were used to investigate the effect of water chemistry on 1,4-dioxane rejection and solute-membrane-solution interaction energy.

##### **4.5.1. Effect of ionic strength**

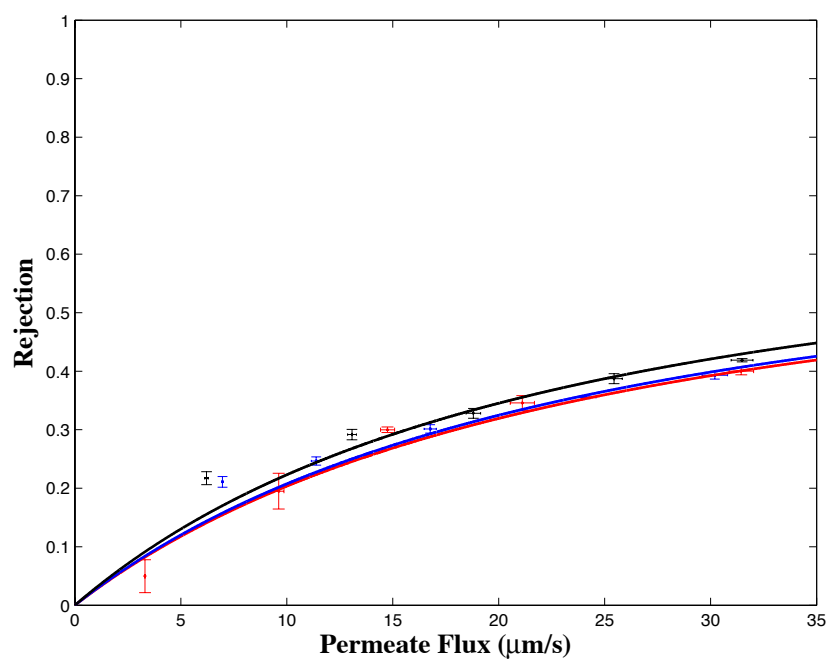
From Figure 4.8, the observed rejections of 1,4-dioxane were around 90% at low permeate flux, then increased slowly with increasing water flux for NF90 and XLE. No difference between three concentrations was observed for all three membranes, which means ionic strength has no significant effect on 1,4-dioxane rejections. Figure 4.7 shows that although NF90 and XLE exhibited large pore size at 500 mM, the membrane structure factor also showed large value, thus validating the explanation of neutralizing polymer charge effect. 1,4-dioxane has larger stokes radius than EG, which is main the reason why 1,4-dioxane showed higher rejection than EG.



(a)



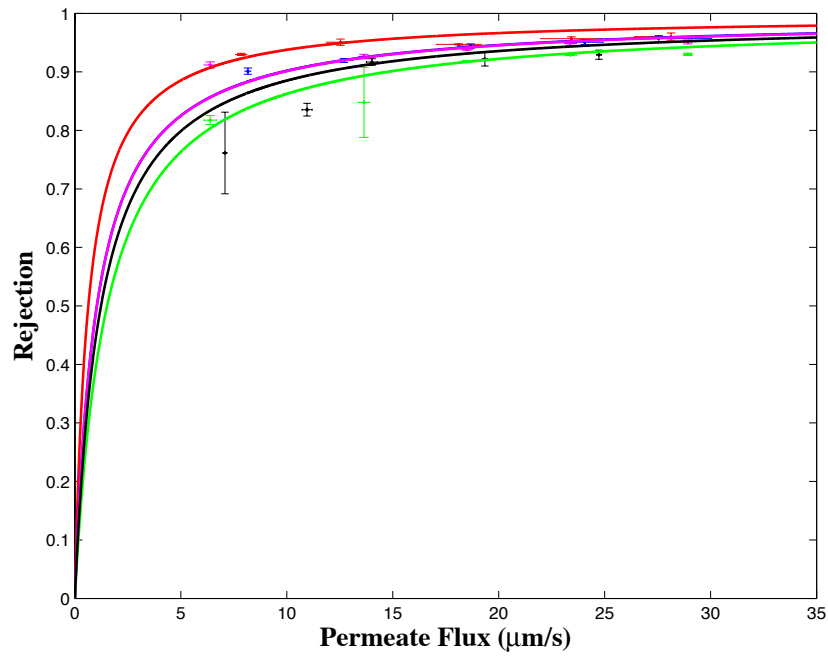
(b)



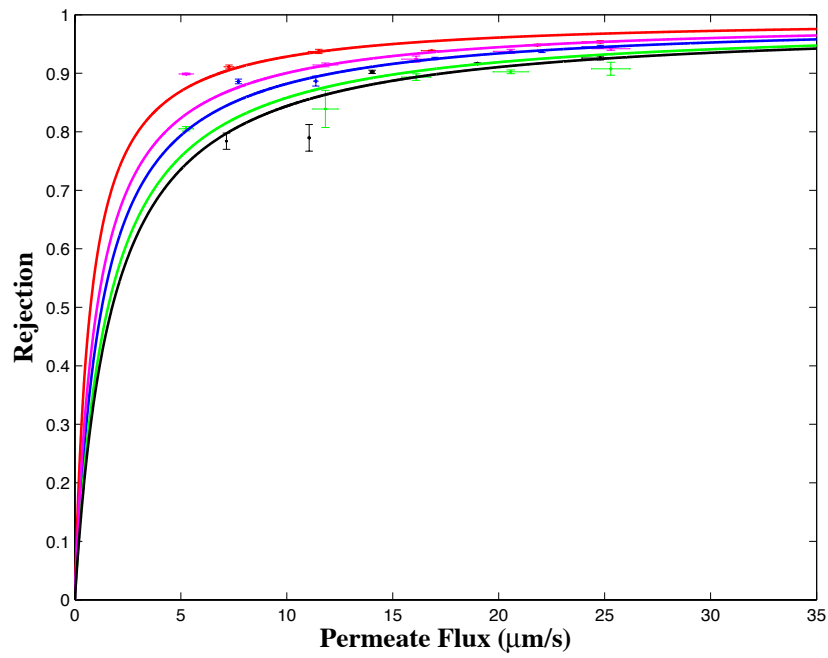
(c)

**Figure 4.8.** 1,4-dioxane real rejection and fitting rejection curves for NF90 (a), XLE (b), NF270 (c) under three concentrations (5 mM=red, 50 mM=blue, 500 mM=black).

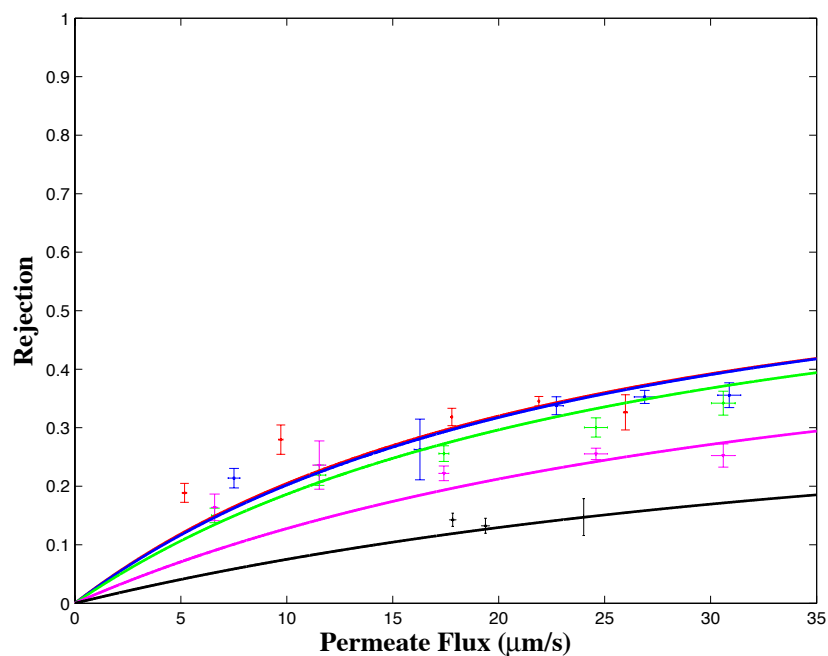
## 4.5.2. Effect of pH



(a)



(b)

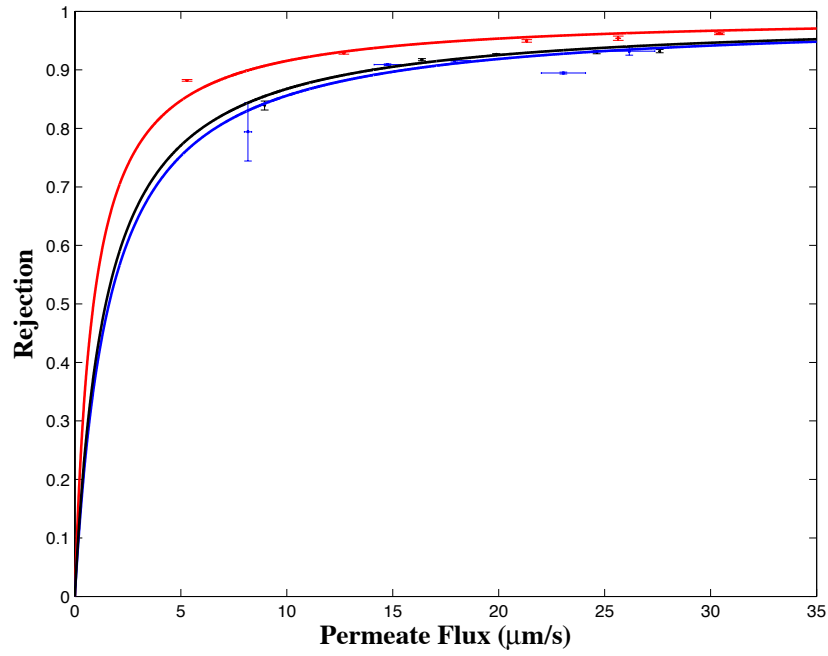


(c)

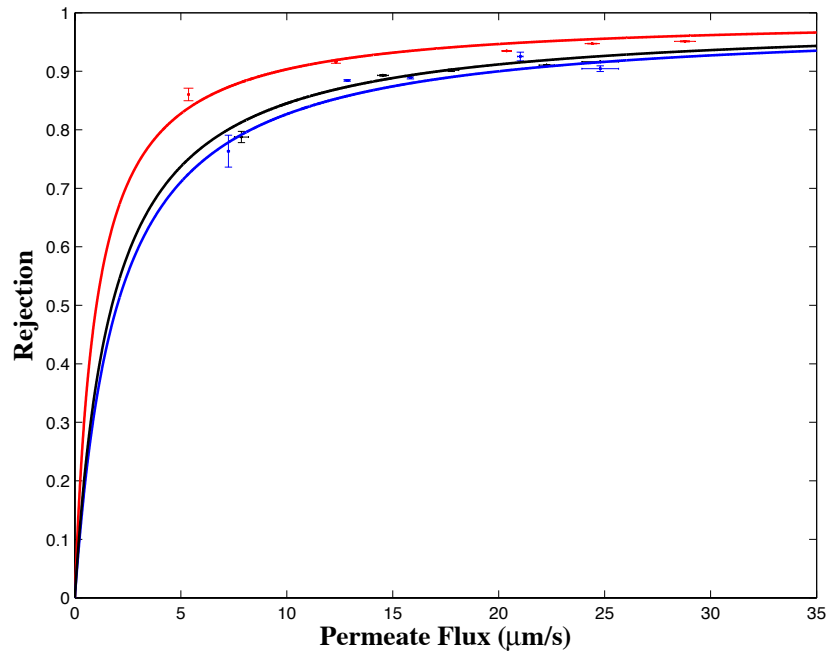
**Figure 4.9.** 1,4-dioxane real rejection and fitting rejection curves for NF90 (a), XLE (b), NF270 (c) under five pH (pH3=red, pH5=blue, pH7=green, pH9=pink, pH11=black).

Figure 4.9 revealed that pH variation did not have significant effect on 1,4-dioxane real rejections for NF90 and XLE, which also is supported by Figure 4.7 that the membrane structure factor varied less than 3% due to pH. However, for NF270, there was an obvious trend that the rejection of 1,4-dioxane decreased with increasing pH from 3 to 11, which may be caused by the enlargement of membrane pore size by 8% as pH increased (Figure 4.7).

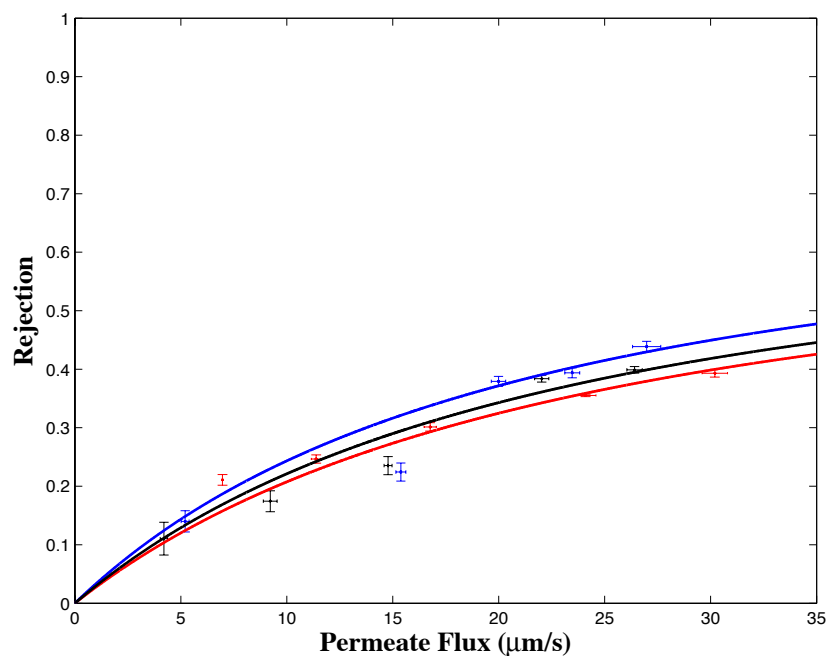
### 4.5.3. Effect of divalent ions



(a)



(b)



(c)

**Figure 4.10.** 1,4-dioxane real rejection and fitting rejection for NF90 (a), XLE (b), NF270 (c) under two divalent ions (50 mM NaCl=red, 50 mM CaCl<sub>2</sub>=blue, 50 mM MgCl<sub>2</sub>=black).

Figure 4.10 indicated that divalent ions reduced the rejection of 1,4-dioxane for NF90 and XLE; NF270 did not show significant difference between divalent ions and monovalent ions. This is consistent with the previous explanation that the membrane pore sizes of NF90 and XLE were enlarged due to larger electrostatic repulsion of divalent ions. NF270 was not sensitive to pore size enlargement because of its relatively low value of  $\lambda$ .

#### 4.5.4. Fitting interaction energy analysis for 1,4-dioxane

Fitting of the interaction energy of 1,4-dioxane (Table 4.5), by inputting the membrane pore size, structure factors and actual 1,4-dioxane rejection curves into the xSDC model. This is the first attempt to calculate the interaction energy of an uncharged organic solute by the xSDC model, which incorporates parameters such as membrane pore size, structural factor, actual rejection and solute size.

**Table 4.5.** Interaction energy for 1,4-dioxane-membrane-water.

Solutions	NF90	NF270	XLE
	$\Delta G_s$ $10^{-21}\text{J}$	$\Delta G_s$ $10^{-21}\text{J}$	$\Delta G_s$ $10^{-21}\text{J}$
NaCl 5 mM	0.39	-4.52	0.65
NaCl 50 mM	3.36	-2.00	2.82
NaCl 500 mM	1.38	-0.54	0.64
NaCl 50 mM,pH=3	0.20	-2.44	0.80
NaCl 50 mM,pH=5	2.77	-2.71	2.25
NaCl 50 mM,pH=7	1.96	-2.85	1.88
NaCl 50 mM,pH=9	3.53	-2.48	3.24
NaCl 50 mM,pH=11	2.76	-2.41	1.48
MgCl <sub>2</sub> 50 mM	2.18	-2.60	1.59
CaCl <sub>2</sub> 50 mM	1.94	-2.02	1.19

NaCl 50 mM was conducted under pH=5.5

Table 4.5 shows that the interaction energy values of NF270 were all negative; it means there is an attraction between 1,4-dioxane and NF270. In other words, NF270 cannot reject 1,4-dioxane very well, which is consistent with what was observed. However, interaction energy is not the dominant factor in membrane performance because the looser membrane structure of NF270 has a greater effect on rejection performance. As the interaction energy of NF270



increased from 5 mM to 500 mM, the membrane pore size was also increasing. Here we may know that the attraction force is reduced as ionic strength increased, that's why the rejection at 500 mM was a little higher than 50 mM and 5 mM for NF270. However, this also could be induced by structural factor increase. Geens et al., [83] found that there is an effective membrane pore radius in membrane-solute interaction, that over a certain membrane pore size, there will always be low membrane-solute interaction.

Interaction energy of NF90 and XLE were similar and showed positive values, which is consistent with the observed membrane structure and rejection curves. From the EG rejection curves for NF90 and XLE, we observed this two membrane showed same rejections and higher rejection than NF270. NF90 and XLE have tighter inter-polymer structure than NF270. NF90 and XLE are made of fully aromatic polyamide, while NF270 is made of semi-aromatic polypiperazine. From the polymer view and contact angle, we know NF90 and XLE are more hydrophobic than NF270. A hydrophilic solute like 1,4-dioxane as will be attracted to a hydrophilic membrane and repelled by hydrophobic membrane, which explains the interaction energy values of NF270 were negative and interaction energy values of NF90, XLE were positive.

**CHAPTER 5**  
**CONCLUSIONS**

## 5. Conclusions

This study focused on the effect of water chemistry on the membrane surface interaction energy, membrane structure, membrane performance, observed uncharged solute (EG and 1,4-dioxane) rejection and water permeability results using the xSDC model. It could be concluded that the membrane pore size and structure factor increases as ionic strength of the feed solution increases. Also, increasing pH enlarges membrane pore size and structure factor and the effect of pH is less significant than ionic strength. Water chemistry has less impact on membrane pore size than membrane structure factor. By calculating membrane structure changes, this research provides supportive evidence regarding membrane transport mechanism to explain variations of membrane performance under different water chemistries. Based on the xSDC model, both steric and chemical interactions determine NF/RO water permeability and organic solute rejection. For the commercial NF/RO membranes tested, solute rejection was most sensitive to pore size within a reasonable range of solute-membrane interaction energies, while water permeability was most sensitive to the membrane structure factor (i.e., effective thickness). Solute-membrane-solution interaction energy also plays an important role in the xSDC model, which characterizes solute partition coefficient through its chemical properties, but its effect is less significant compared to the membrane structure. The xSDC model is a useful tool, which may help to reveal more fundamental, mechanistic insights into the relationship between membrane structure, chemistry and performance, and ultimately, to make better membranes tailored to different water treatment applications.

## References

- [1] A. Verliefde, Rejection of Organic Micropollutants by High Pressure Membrane (NF/RO), Water Management Academic Press, Delft, 2008.
- [2] J.-M. Davies, A. Mazumder, Health and environmental policy issues in Canada: the role of watershed management in sustaining clean drinking water quality at surface sources, *Journal of Environmental Management*, 68 (2003) 273-286.
- [3] CDPH, NDMA and Other Nitrosamines - Drinking Water Issues, in, 2011.
- [4] P.G. Thomas K. G. Mohr, 1,4-Dioxane and other solvent stabilizers, in: S.C.V.W. District (Ed.), Santa Clara, 2001.
- [5] G.-G. Ying, R.S. Kookana, Y.-J. Ru, Occurrence and fate of hormone steroids in the environment, *Environment International*, 28 (2002) 545-551.
- [6] K.G. Babi, K.M. Koumenides, A.D. Nikolaou, C.A. Makri, F.K. Tzoumerkas, T.D. Lekkas, Pilot study of the removal of THMs, HAAs and DOC from drinking water by GAC adsorption, *Desalination*, 210 (2007) 215-224.
- [7] J. Kim, B. Kang, DBPs removal in GAC filter-adsorber, *Water Research*, 42 (2008) 145-152.
- [8] L.N. Nguyen, F.I. Hai, J. Kang, W.E. Price, L.D. Nghiem, Removal of trace organic contaminants by a membrane bioreactor, granular activated carbon (MBR, GAC) system, *Bioresource Technology*, 113 (2012) 169-173.
- [9] P. Westerhoff, H. Moon, D. Minakata, J. Crittenden, Oxidation of organics in retentates from reverse osmosis wastewater reuse facilities, *Water Research*, 43 (2009) 3992-3998.
- [10] K. Ito, W. Jian, W. Nishijima, A.U. Baes, E. Shoto, M. Okada, Comparison of ozonation and AOPs combined with biodegradation for removal of THM precursors in treated sewage effluents, *Water Science and Technology*, 38 (1998) 179-186.
- [11] R. Broseus, S. Vincent, K. Aboulfadl, A. Daneshvar, S. Sauve, B. Barbeau, M. Prevost, Ozone oxidation of pharmaceuticals, endocrine disruptors and pesticides during drinking water

treatment, *Water Research*, 43 (2009) 4707-4717.

[12] S. Chowdhury, P. Champagne, P.J. McLellan, Models for predicting disinfection byproduct (DBP) formation in drinking waters: A chronological review, *Science of The Total Environment*, 407 (2009) 4189-4206.

[13] M.H. Plumlee, M. Lopez-Mesas, A. Heidelberger, K.P. Ishida, M. Reinhard, N-nitrosodimethylamine (NDMA) removal by reverse osmosis and UV treatment and analysis via LC, *MS/MS*, *Water Research*, 42 (2008) 347-355.

[14] C.M. Sharpless, C.I. Chou, A.A. Mofidi, K.G. Linden, N-Nitrosodimethylamine Removal From Drinking Water by UV-Treatment: A Direct Comparison of Different UV Technologies, in: *American Water Works Association*, Washington, 01-Jan-2001.

[15] J.C. Kruithof, P.C. Kamp, B.J. Martijn, UV/H<sub>2</sub>O<sub>2</sub> Treatment: A Practical Solution for Organic Contaminant Control and Primary Disinfection, *Ozone: Science & Engineering*, 29 (2007) 273-280.

[16] Y. Yoon, R.M. Lueptow, Removal of organic contaminants by RO and NF membranes, *Journal of Membrane Science*, 261 (2005) 76-86.

[17] C. Bellona, J.E. Drewes, P. Xu, G. Amy, Factors affecting the rejection of organic solutes during NF/RO treatment, *A literature review*, *Water Research*, 38 (2004) 2795-2809.

[18] A. Jawor, E.M.V. Hoek, Effects of feed water temperature on inorganic fouling of brackish water RO membranes, *Desalination*, 235 (2009) 44-57.

[19] G. Hurwitz, G.R. Guillen, E.M.V. Hoek, Probing polyamide membrane surface charge, zeta potential, wettability, and hydrophilicity with contact angle measurements, *Journal of Membrane Science*, 349 (2010) 349-357.

[20] A.R.D. Verliefde, E.R. Cornelissen, S.G.J. Heijman, E.M.V. Hoek, G.L. Amy, B.V.d. Bruggen, J.C. van Dijk, Influence of Solute-Membrane Affinity on Rejection of Uncharged Organic Solutes by Nanofiltration Membranes, *Environmental Science & Technology*, 43 (2009) 2400-2406.

- [21] A.R.D. Verliefde, E.R. Cornelissen, S.G.J. Heijman, J.Q.J.C. Verberk, G.L. Amy, B. Van der Bruggen, J.C. van Dijk, The role of electrostatic interactions on the rejection of organic solutes in aqueous solutions with nanofiltration, *Journal of Membrane Science*, 322 (2008) 52-66.
- [22] Factors Affecting RO membrane Performance, in: *F. membranes (Ed.)*, Dow, 1998.
- [23] T. Fujioka, L.D. Nghiem, S.J. Khan, J.A. McDonald, Y. Poussade, J.E. Drewes, Effects of feed solution characteristics on the rejection of N-nitrosamines by reverse osmosis membranes, *Journal of Membrane Science*, 409, 410 (2012) 66-74.
- [24] A.E. Childress, M. Elimelech, Relating Nanofiltration Membrane Performance to Membrane Charge (Electrokinetic) Characteristics, *Environmental Science & Technology*, 34 (2000) 3710-3716.
- [25] S. Chowdhury, M.J. Rodriguez, J. Serodes, Model development for predicting changes in DBP exposure concentrations during indoor handling of tap water, *Science of The Total Environment*, 408 (2010) 4733-4743.
- [26] A.M. Comerton, R.C. Andrews, D.M. Bagley, Evaluation of an MBR, RO system to produce high quality reuse water: Microbial control, DBP formation and nitrate, *Water Research*, 39 (2005) 3982-3990.
- [27] X. Yang, C. Shang, W. Lee, P. Westerhoff, C. Fan, Correlations between organic matter properties and DBP formation during chloramination, *Water Research*, 42 (2008) 2329-2339.
- [28] J.-B. Serodes, M.J. Rodriguez, H. Li, C. Bouchard, Occurrence of THMs and HAAs in experimental chlorinated waters of the Quebec City area (Canada), *Chemosphere*, 51 (2003) 253-263.
- [29] Trihalomethanes: Health Information Summary, in: *N.H.D.o.E. Services (Ed.)*, New Hampshire 03301, 2006.
- [30] U.S.E.P. Agency, Basic Information about Disinfection Byproducts in Drinking Water: Total Trihalomethanes, Haloacetic Acids, Bromate, and Chlorite, in, EPA, 2012.

[31] J. Choi, R.L. Valentine, Formation of N-nitrosodimethylamine (NDMA) from reaction of monochloramine: a new disinfection by-product, *Water Research*, 36 (2002) 817-824.

[32] OEHHA, Public health goals for chemicals in drinking water, N-Nitrosodimethylamine, in, 2006.

[33] U.S.EP. Agency, Analytical method development for the analysis of N-nitrosodimethylamine(NDMA) in drinking water, in, 2005.

[34] U.S.EP. Agency, Fact Sheet: Final Third Drinking Water Contaminant Candidate List (CCL 3), in: EPA (Ed.), 2009.

[35] B.J. Richardson, P.K.S. Lam, M. Martin, Emerging chemicals of concern: Pharmaceuticals and personal care products (PPCPs) in Asia, with particular reference to Southern China, *Marine Pollution Bulletin*, 50 (2005) 913-920.

[36] U.S.EP. Agency, Pharmaceuticals and Personal Care Products as Pollutants (PPCPs), in, EPA, 2012.

[37] M.C. Sonia Suárez., Francisco Omil., Juan M. Lema, How are pharmaceutical and personal care products (PPCPs) removed from urban wastewaters?, *Reviews in Environmental Science and Biotechnology*, 7(2) (2008) 125-138.

[38] T.C.G. Kibbey, L. Chen, N. Singhaputtangkul, D.A. Sabatini, A UV-transparent passive concentrator/spectrum deconvolution method for simultaneous detection of endocrine disrupting chemicals (EDCs) and related contaminants in natural waters, *Chemosphere*, 76 (2009) 1249-1257.

[39] P.D. Hansen, H. Dizer, B. Hock, A. Marx, J. Sherry, M. McMaster, C. Blaise, Vitellogenin, À a biomarker for endocrine disruptors, *TrAC Trends in Analytical Chemistry*, 17 (1998) 448-451.

[40] H.-S. Chang, K.-H. Choo, B. Lee, S.-J. Choi, The methods of identification, analysis, and removal of endocrine disrupting compounds (EDCs) in water, *Journal of Hazardous Materials*, 172 (2009) 1-12.

[41] R.M. Sharpe, N.E. Skakkebaek, Are oestrogens involved in falling sperm counts and disorders of the male reproductive tract?, *The Lancet*, 341 (1993) 1392-1396.

[42] U.S.E.P. Agency, Polychlorinated Biphenyls (PCBs), in, EPA, 2012.

[43] Y. Zhang, Y. Mu, J. Liu, A. Mellouki, Levels, sources and health risks of carbonyls and BTEX in the ambient air of Beijing, China, *Journal of Environmental Sciences*, 24 (2012) 124-130.

[44] W.H. Organization, Air Quality Guidelines for Europe. WHO Regional Publication, European Series. World Health Organization, Regional Office for Europe, in: WHO (Ed.), 1999.

[45] U.S.E.P. Agency, 2011 Edition of the Drinking Water Standards and Health Advisories, in: EPA (Ed.), Washington,DC, 2011.

[46] H. Alomirah, S. Al-Zenki, S. Al-Hooti, S. Zaghloul, W. Sawaya, N. Ahmed, K. Kannan, Concentrations and dietary exposure to polycyclic aromatic hydrocarbons (PAHs) from grilled and smoked foods, *Food Control*, 22 (2011) 2028-2035.

[47] G. Environmental, GSI CHEMICAL PROPERTIES DATABASE, in, GSI.

[48] P.Ç. Andrzejewski, B. Kasprzyk-Hordern, J. Nawrocki, The hazard of N-nitrosodimethylamine (NDMA) formation during water disinfection with strong oxidants, *Desalination*, 176 (2005) 37-45.

[49] H. Nourmoradi, M. Nikaeen, M. Khiadani, Removal of benzene, toluene, ethylbenzene and xylene (BTEX) from aqueous solutions by montmorillonite modified with nonionic surfactant: Equilibrium, kinetic and thermodynamic study, *Chemical Engineering Journal*, 191 (2012) 341-348.

[50] CP. Silva, M. Otero, V. Esteves, Processes for the elimination of estrogenic steroid hormones from water: A review, *Environmental Pollution*, 165 (2012) 38-58.

[51] K. Kimura, G. Amy, Jr.E. Drewes, T. Heberer, T.-U. Kim, Y. Watanabe, Rejection of organic micropollutants (disinfection by-products, endocrine disrupting compounds, and pharmaceutically active compounds) by NF/RO membranes, *Journal of Membrane Science*, 227



(2003) 113-121.

[52] J.L.C. Santos, P. de Beukelaar, I.F.J. Vankelecom, S. Velizarov, J.G. Crespo, Effect of solute geometry and orientation on the rejection of uncharged compounds by nanofiltration, *Separation and Purification Technology*, 50 (2006) 122-131.

[53] M.J. Ariza, A. Canas, J. Malfeito, J. Benavente, Effect of pH on electrokinetic and electrochemical parameters of both sub-layers of composite polyamide/polysulfone membranes, *Desalination*, 148 (2002) 377-382.

[54] C.M. Nguyen, S. Bang, J. Cho, K.-W. Kim, Performance and mechanism of arsenic removal from water by a nanofiltration membrane, *Desalination*, 245 (2009) 82-94.

[55] M.H. Oo, L. Song, Effect of pH and ionic strength on boron removal by RO membranes, *Desalination*, 246 (2009) 605-612.

[56] J. Yang, S. Lee, E. Lee, J. Lee, S. Hong, Effect of solution chemistry on the surface property of reverse osmosis membranes under seawater conditions, *Desalination*, 247 (2009) 148-161.

[57] T. Hoang, G. Stevens, S. Kentish, The effect of feed pH on the performance of a reverse osmosis membrane, *Desalination*, 261 (2010) 99-103.

[58] C. Bartels, R. Franks, S. Rybar, M. Schierach, M. Wilf, The effect of feed ionic strength on salt passage through reverse osmosis membranes, *Desalination*, 184 (2005) 185-195.

[59] X. Jin, X. Huang, E.M.V. Hoek, Role of Specific Ion Interactions in Seawater RO Membrane Fouling by Alginic Acid, *Environmental Science & Technology*, 43 (2009) 3580-3587.

[60] M.E. Williams, A Review of Reverse Osmosis Theory, in, EET Corporation and Williams Engineering Services Company, Inc., 2003.

[61] M.A. Mazid, Mechanisms of Transport Through Reverse Osmosis Membranes, *Separation Science and Technology*, 19,357 (1984).

- [62] M. Kargol, A. Kargol, Mechanistic equations for membrane substance transport and their identity with Kedem, Katchalsky equations, *Biophysical Chemistry*, 103 (2003) 117-127.
- [63] Z. Kovacs, M. Discacciati, W. Samhaber, Modeling of amino acid nanofiltration by irreversible thermodynamics, *Journal of Membrane Science*, 332 (2009) 38-49.
- [64] M. Jarzynska, M. Pietruszka, The application of the Kedem, Katchalsky equations to membrane transport of ethyl alcohol and glucose, *Desalination*, 280 (2011) 14-19.
- [65] K.S. Spiegler, O. Kedem, Thermodynamics of hyperfiltration (reverse osmosis): criteria for efficient membranes, *Desalination*, 1 (1966) 311-326.
- [66] P. Fubing, H. Xiaofei, A. Jawor, E.M.V. Hoek, Transport, structural, and interfacial properties of poly(vinyl alcohol)polysulfone composite nanofiltration membranes, *Journal of Membrane Science*, 353 (2010) 169-176.
- [67] E.M.V. Hoek, A.S. Kim, M. Elimelech, Influence of crossflow membrane filter geometry and shear rate on colloidal fouling in reverse osmosis and nanofiltration separations, *Environmental Engineering Science*, 19 (2002) 357-372.
- [68] J. Wang, E.M.V. Hoek, A Facile Structure-Performance Model for Transport through NF/RO Membranes. In Preparation., (2011).
- [69] S. Bhattacharjee, A. Sharma, P.K. Bhattacharya, Estimation and Influence of Long Range Solute. Membrane Interactions in Ultrafiltration, *Industrial & Engineering Chemistry Research*, 35 (1996) 3108-3121.
- [70] P.M. Bungay, H. Brenner, The motion of a closely-fitting sphere in a fluid-filled tube, *International Journal of Multiphase Flow*, 1 (1973) 25-56.
- [71] C.J. van Oss, Development and applications of the interfacial tension between water and organic or biological surfaces, *Colloids and Surfaces B: Biointerfaces*, 54 (2007) 2-9.
- [72] L.D. Nghiem, A.I. Schafer, M. Elimelech, Removal of Natural Hormones by Nanofiltration Membranes: Measurement, Modeling, and Mechanisms, *Environmental Science & Technology*, 38 (2004) 1888-1896.

- [73] A. Carvalho, F. Maugeri, V. Silva, A. Hernández, L. Palacio, P. Pradanos, AFM analysis of the surface of nanoporous membranes: application to the nanofiltration of potassium clavulanate, *Journal of Materials Science*, 46 (2011) 3356-3369.
- [74] K.V. Plakas, A.J. Karabelas, Membrane retention of herbicides from single and multi-solute media: The effect of ionic environment, *Journal of Membrane Science*, 320 (2008) 325-334.
- [75] G. Wypych, *A Properties Database*, in: ChemTec Publishing, New York, 2000.
- [76] H. Canada, Canadian Environmental Protection Act — Priority Substances List — Supporting document for the health assessment of ethylene glycol., in: E.H. Directorate (Ed.), Bureau of Chemical Hazards, Ottawa, Ontario, 2000.
- [77] ChemIDplus., National Library of Medicine, in, ChemIDplus Advanced, 2009.
- [78] Braghetta, F. DiGiano, Ball, Nanofiltration of Natural Organic Matter: pH and Ionic Strength Effects, *Journal of Environmental Engineering*, 123 (1997) 628-641.
- [79] Pei Xu, Jörg E. Drewes, Christopher Bellona, Gary Amy, Tae-Uk Kim, Marc Adam, T. Heberer, Rejection of Emerging Organic Micropollutants in Nanofiltration–Reverse Osmosis Membrane Applications, *Water Environment Research*, 77 (2005) 40-48(49).
- [80] C. Bellona, J.r.E. Drewes, P. Xu, G. Amy, Factors affecting the rejection of organic solutes during NF/RO treatment, A literature review, *Water Research*, 38 (2004) 2795-2809.
- [81] M. Manttari, A. Pihlajamaki, M. Nystrom, Effect of pH on hydrophilicity and charge and their effect on the filtration efficiency of NF membranes at different pH, *Journal of Membrane Science*, 280 (2006) 311-320.
- [82] S.S. Deshmukh, A.E. Childress, Zeta potential of commercial RO membranes: influence of source water type and chemistry, *Desalination*, 140 (2001) 87-95.
- [83] J. Geens, A. Hillen, B. Bettens, B. Van der Bruggen, C. Vandecasteele, Solute transport in non-aqueous nanofiltration: effect of membrane material, *Journal of Chemical Technology & Biotechnology*, 80 (2005) 1371-1377.

